DEPARTMENT OF DEFENCE
DEFENCE SCIENCE & TECHNOLOGY ORGANISATION
DSTO

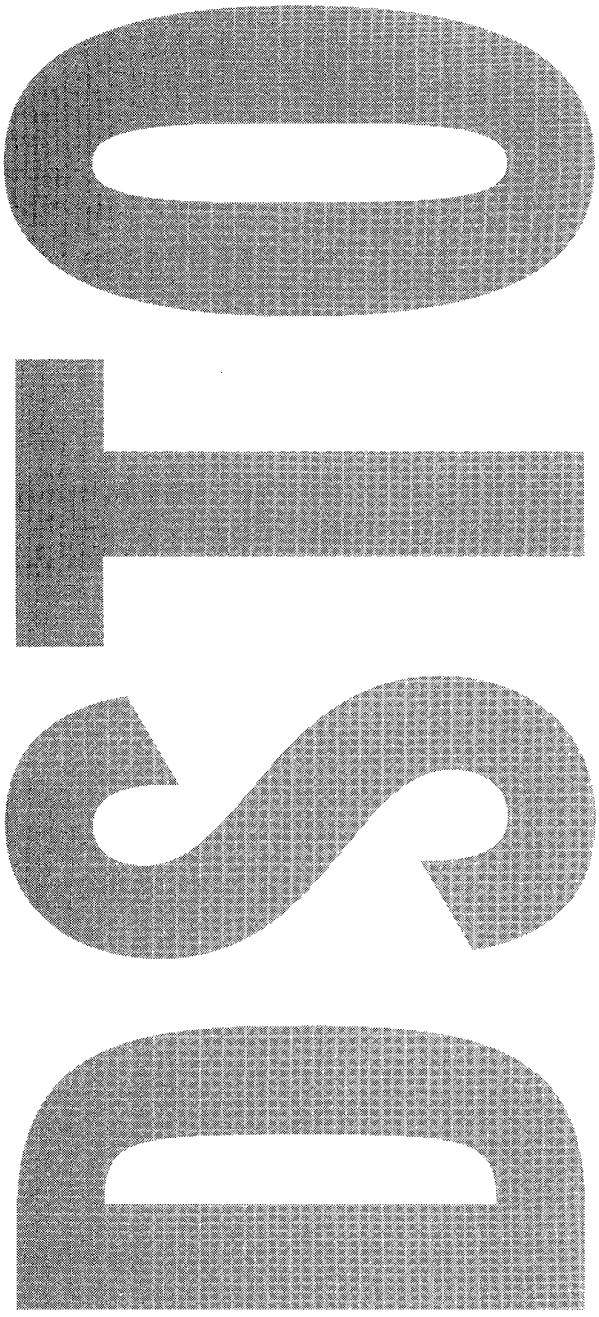

Inverting the Circular Radon Transform

Nicholas J. Redding and
Garry N. Newsam

DSTO-RR-0211

Inverting the Circular Radon Transform

Nicholas J. Redding and Garry N. Newsam

Surveillance Systems Division
Electronics and Surveillance Research Laboratory

DSTO–RR–0211

ABSTRACT

In this report we show how image formation or reconstruction in synthetic aperture radar (SAR) can be viewed as the inversion of the circular Radon transform. The advantage of viewing image formation in this way is that it could be used in situations where more standard methods could fail such as high squint and ultra-wideband SAR. We examine previous work in the literature on circular Radon transforms and their inversion. Next, we present some novel techniques and analytic expressions for the transform of some key functions. We briefly consider motion compensation. Finally, we propose a number of possible methods that could be pursued to make new practical image formation algorithms.

Published by

DSTO Electronics and Surveillance Research Laboratory
PO Box 1500
Edinburgh, South Australia, Australia 5111

Telephone: (08) 8259 5555
Facsimile: (08) 8259 6567

AR No. 011-855
August, 2001

APPROVED FOR PUBLIC RELEASE

Inverting the Circular Radon Transform

EXECUTIVE SUMMARY

The Radon transform is an integral along a path, and in its simplest form this path is a straight line. We will refer to this form of the transform as the normal Radon transform (NRT) because it is usually written using the normal equation for the line. Jakowatz *et al.* (based on work by Munson *et al.*) showed the relationship between this line integral and spotlight SAR image formation using the polar-to-rectangular resampling process. This corresponds to the Fresnel approximation to the wavefront: the radiating energy from the radar is assumed to be planar. However, this approximation only holds in restricted physical geometries and limits the size and resolution of the image that can be formed.

In reality, the wavefront radiating from the radar's antenna is spherical, with the sector of the sphere determined by the antenna beam pattern and geometry. As a consequence, the received signal at a particular antenna position and time since transmission is an average (integral) of the surface reflectivity (at the radiation's frequency) at all points where the spherical wavefront impinged upon the ground at half that time (to account for the round trip). We will ignore the effect of shape and duration of the transmitted pulse by assuming that the received data has been range compressed by matched filtering the received signal against the transmitted pulse. The antenna position is usually a function of time along a straight line, and so this coordinate is referred to as *slow time.* In contrast, the time interval between transmission and reception of a pulse corresponding to a particular range is referred to as *fast time.*

If the geometry of the imaged terrain is planar, the locus of its intersection with the spherical wavefront will be the arc of a circle. Under this assumption, the received radar signal is an average of the ground reflectivity over a circular arc. Consequently, the radar performs a circular Radon transform (CRT) of the ground reflectivity. Therefore, forming an image of the ground reflectivity in synthetic aperture radar (SAR) is the process of inverting the circular averages, or in other words, inverting the circular Radon transform of the received radar signal. This approach to image formation provides an alternative view to understanding the SAR image formation process and can be used to develop algorithms that are free of the range curvature limitations of standard techniques. The approach used here may also be more intuitive for many readers unfamiliar with radar, because the concepts of doppler and phase are not required. In addition, methods based on inverting the CRT could be used in situations where the more standard techniques may fail because the stationary phase approximation is inappropriate, such as ultra-wideband or foliage penetration SAR, and high-squint SAR for tactical platforms. Follow-on work however will be needed to determine the practical utility of the results presented here.

In this report we examine the existing body of literature on inverting the CRT and related methods in the SAR literature. In addition, we present a number of new methods for inverting the CRT as the basis for future research. We assume that the radar is monostatic (co-located transmitter and receiver), and that the propagation medium is isotropic, homogeneous and non-dispersive so that the wave velocity is constant in space. Then using the Born approximation, the radar echo is assumed to be a sum of single-

scattering objects. We also use the "start-stop" approximation because the sensor platform speed is much less than the wave velocity. Furthermore, we make three assumptions that can be removed at the cost of complexity. Firstly, the geometry is assumed to be two-dimensional, *i.e.* we can ignore the height of the radar above the ground plane. Secondly, the illumination of the ground by the antenna in both transmission and reception is assumed to be uniform. Finally, we assume an aspect independent ground reflectivity.

This work was carried out while the first author was on attachment to the Defence Evaluation & Research Agency, Malvern UK.

Authors

Nicholas J. Redding
Surveillance Systems Division

Nicholas Redding received a B.E. and Ph.D. in electrical engineering all from the University of Queensland, Brisbane, in 1986 and 1991, respectively. From 1988 he received a Research Scientist Fellowship from the Australian Defence Science and Technology Organisation (DSTO) and then joined DSTO in Adelaide as a Research Scientist after completing his Ph.D. in artificial neural networks in 1991. In 1996 he was appointed as a Senior Research Scientist in the Microwave Radar Division (now Surveillance Systems Division) of DSTO. Since joining DSTO he has applied image processing techniques to the automatic classification of ionospheric data, and more recently has researched target detection (both human and algorithmic) in synthetic aperture radar imagery. He is currently on a one year posting to the UK's Defence Evaluation and Research Agency.

Garry N. Newsam
Surveillance Systems Division

Garry Newsam received a B.Sc. and M.Sc. in mathematics from the University of Canterbury, New Zealand in 1978, and an A.M. and Ph.D. in applied mathematics from Harvard University in 1983. He then worked for a year as a research fellow at Victoria University, New Zealand examining the statistics of energy use in commercial buildings. After this he joined the Centre for Mathematical Analysis at the Australian National University as a research fellow and lecturer: there he taught and did theoretical and applied work on inverse problems in optics, atmospheric chemistry and groundwater modelling.

Since 1995 Dr Newsam has been a Principal Research Scientist with DSTO, leading a group now within Surveillance Systems Division tackling problems in image analysis and related areas. His current research interests include image processing and compression, spline fitting and image registration, reconstructing shapes from imagery, modelling and generating random fields, and Radon transforms.

Contents

Figures

Tables

1 Introduction

The Radon transform is an integral along a path, and in its simplest form this path is a straight line. We will refer to this form of the transform as the normal Radon transform (NRT) because it is usually written using the normal equation for the line. Jakowatz *et al.* [18] (based on work by Munson *et al.* [23]) showed the relationship between this line integral and spotlight SAR image formation using the polar-to-rectangular resampling process. This corresponds to the Fresnel approximation to the wavefront: the radiating energy from the radar is assumed to be planar. However, this approximation only holds in restricted physical geometries and limits the size and resolution of the image that can be formed [18].

In reality, the wavefront radiating from the radar's antenna is spherical, with the sector of the sphere determined by the antenna beam pattern and geometry. As a consequence, the received signal at a particular antenna position and time since transmission is an average (integral) of the surface reflectivity (at the radiation's frequency) at all points where the spherical wavefront impinged upon the ground at half that time (to account for the round trip). We will ignore the effect of shape and duration of the transmitted pulse by assuming that the received data has been range compressed by matched filtering the received signal against the transmitted pulse (see Section 3.1). The antenna position is usually a function of time along a straight line, and so this coordinate is referred to as *slow time*. In contrast, the time interval between transmission and reception of a pulse corresponding to a particular range is referred to as *fast time*.

If the geometry of the imaged terrain is planar, the locus of its intersection with the spherical wavefront will be the arc of a circle. Under this assumption, the received radar signal is an average of the ground reflectivity over a circular arc. Consequently, the radar performs a circular Radon transform (CRT) of the ground reflectivity. Therefore, forming an image of the ground reflectivity in synthetic aperture radar (SAR) is the process of inverting the circular averages, or in other words, inverting the circular Radon transform of the received radar signal. This approach to image formation provides an alternative view to understanding the SAR image formation process and can be used to develop algorithms that are free of the range curvature limitations of standard techniques. The approach used here may also be more intuitive for many readers unfamiliar with radar, because the concepts of doppler and phase are not required [18, 22, 2]. In addition, methods based on inverting the CRT could be used in situations where the more standard techniques may fail because the stationary phase approximation [32] is inappropriate, such as ultra-wideband or foliage penetration SAR [16], and high-squint SAR for tactical platforms. Follow-on work however will be needed to determine the practical utility of the results presented here.

In this report we examine the existing body of literature on inverting the CRT and related methods in the SAR literature. In addition, we present a number of new methods for inverting the CRT as the basis for future research. Like [36], we assume that the radar is monostatic (co-located transmitter and receiver), and that the propagation medium is isotropic, homogeneous and non-dispersive so that the wave velocity is constant in space. Then using the Born approximation, the radar echo is assumed to be a sum of single-scattering objects. We also use the "start-stop" approximation because the sensor platform

speed is much less than the wave velocity. Furthermore, we make three assumptions that can be removed at the cost of complexity. Firstly, the geometry is assumed to be two-dimensional, *i.e.* we can ignore the height of the radar above the ground plane. Secondly, the illumination of the ground by the antenna in both transmission and reception is assumed to be uniform. Finally, we assume an aspect independent ground reflectivity.

In the next section we review the basics of the normal Radon transform as a starting point for our development of the CRT. Because the CRT is a generalisation of the NRT, many of the concepts relevant to both can be presented more simply in the context of the NRT using well-established theory. Having established the basic Radon transform theory, we then briefly consider some established SAR image reconstruction methods in Section 3 to set the linkage with the received radar signal. Section 4 states the inverse CRT in concise terms, and Section 5 examines previous methods for determining the inverse CRT, including the link to the well-known range migration algorithm for SAR image formation. Section 6 presents some new Fourier resampling methods for the ICRT, Section 7 derives properties of the CRT and inverse CRT, and Section 8 discusses various options for new practical methods for SAR image formation. Section 9 briefly discusses motion compensation, and conclusions are presented in Section 10.

2 Radon Transform and its Inverse

2.1 Normal Radon Transform

Typically, the Radon transform of the function $f(x,y)$, $x,y \in \mathbb{R}$, is defined as a path integral along a straight line of the function,

$$g(\rho,\theta) = (\mathcal{R}f)(\rho,\theta) = \int_{-\infty}^{\infty}\int_{-\infty}^{\infty} f(x,y)\delta(\rho - x\cos\theta - y\sin\theta)\,dx\,dy, \tag{1}$$

where $\delta(\cdot)$ is the Dirac delta function and (ρ,θ) are the parameters of a normal equation for the line of integration. (See [28] for the algebra of the Dirac delta function.)

Several different approaches exist for inverting the Radon transform. The first one we will consider employs the Projection Slice Theorem [18], which states that the one-dimensional Fourier transform of any projection $p_\theta(\rho) = (\mathcal{R}f)(\rho,\theta)$ is equal to the two-dimensional Fourier transform with respect to the polar coordinates of the image $f(x,y)$ to be reconstructed, *i.e.*

$$F(\nu\cos\theta, \nu\sin\theta) = P_\theta(\nu), \tag{2}$$

where

$$\begin{aligned} F(k_x,k_y) &= \int_{-\infty}^{\infty}\int_{-\infty}^{\infty} f(x,y)e^{2\pi i(xk_x+yk_y)}\,dx\,dy, \\ P_\theta(\nu) &= \int_{-\infty}^{\infty} p_\theta(\rho)e^{2\pi i\rho\nu}\,d\rho. \end{aligned} \tag{3}$$

Consequently, by (2), we may invert the Radon transform by use of one-dimensional and two-dimensional Fourier transforms. The standard Fast Fourier Transform (FFT) on

a uniform grid can be employed if a polar to rectangular coordinate transformation is undertaken [18, 34]; otherwise non-uniformly sampled FFT techniques must be employed [3, 4, 11, 29, 33, 37]. Note that the theorem can be used in reverse order to calculate the Radon transform of a signal $f(x, y)$.

Filtered backprojection is probably the most commonly used approach to inverting the Radon transform. It is derived as follows. Starting with the inverse of (3),

$$f(x,y) = \int_{-\infty}^{\infty}\int_{-\infty}^{\infty} F(k_x,k_y)e^{-2\pi i(xk_x+yk_y)}\,dk_x\,dk_y$$

and converting to polar coordinates we obtain [34]

$$\begin{aligned} f(x,y) &= \int_0^{2\pi}\int_0^{\infty} \nu F(\nu\cos\theta,\nu\sin\theta)e^{-2\pi i\nu(x\cos\theta+y\sin\theta)}\,d\nu\,d\theta \\ &= \int_0^{\pi}\int_{-\infty}^{\infty} |\nu| F(\nu\cos\theta,\nu\sin\theta)e^{-2\pi i\nu(x\cos\theta+y\sin\theta)}\,d\nu\,d\theta \\ &= \int_0^{\pi}\int_{-\infty}^{\infty} |\nu| \left(\int_{-\infty}^{\infty} p_\theta(\rho)e^{2\pi i\rho\nu}\,d\rho\right) e^{-2\pi i\nu(x\cos\theta+y\sin\theta)}\,d\nu\,d\theta. \end{aligned} \tag{4}$$

Typically, (4) is written as two steps, the first of which is a high-pass filtering step in the frequency domain,

$$\hat{p}_\theta(\rho) = \int_{-\infty}^{\infty} |\nu| \left(\int_{-\infty}^{\infty} p_\theta(\rho)e^{2\pi i\rho\nu}\,d\rho\right) e^{-2\pi i\rho\nu}\,d\nu, \tag{5}$$

followed by integration of the set of projections $\hat{g}(\rho,\theta) = \hat{p}_\theta(\rho)$,

$$\begin{aligned} f(x,y) &= \int_0^{\pi} \hat{g}(x\cos\theta + y\sin\theta,\theta)\,d\theta \\ &= \int_0^{\pi}\int_{-\infty}^{\infty} \hat{g}(\rho,\theta)\delta(\rho - x\cos\theta - y\sin\theta)\,d\rho\,d\theta, \end{aligned} \tag{6}$$

which is called backprojection and is simply an integration along sinusoidal paths of the filtered projections $\hat{g}(\rho,\theta)$.

It can be shown that the backprojection operation is equal to half the adjoint Radon transform [9]. To see this, firstly let $g(\rho,\theta)$ be the normal Radon transform of some function, then we define the backprojection operator $\mathcal{B}$ by

$$(\mathcal{B}g)(x,y) = \int_0^{\pi} g(x\cos\theta + y\sin\theta,\theta)\,d\theta. \tag{7}$$

Then by the symmetry property $g(\rho,\theta) = g(-\rho,-\theta)$ and

$$\begin{aligned} (\mathcal{B}g)(x,y) &= \frac{1}{2}\int_0^{2\pi} g(x\cos\theta + y\sin\theta,\theta)\,d\theta \\ &= \frac{1}{2}(\mathcal{R}^\dagger g)(x,y), \end{aligned} \tag{8}$$

where $\mathcal{R}^\dagger g$ is the adjoint normal Radon transform.

We can see that $\mathcal{R}^\dagger$ is the adjoint operator from the following development [9]. Firstly, let $\langle \cdot, \cdot \rangle$ designate an inner product in $\mathbb{R}^2$, and in the transform domain let $\langle \cdot, \cdot \rangle_p$ designate an inner product in $\mathbb{R} \times [0, 2\pi]$. Secondly, let $f(\mathbf{x})$ and $h(\mathbf{x})$, $\mathbf{x} \in \mathbb{R}^2$, be C^∞ functions, and $g(\rho, \theta) = \mathcal{R}f(\mathbf{x})$. Then

$$\begin{aligned}
\langle h, \mathcal{R}^\dagger g \rangle &= \int_{\mathbb{R}^2} h(\mathbf{x})(\mathcal{R}^\dagger g)(\mathbf{x})\, d\mathbf{x} \\
&= \int_{\mathbb{R}^2} h(\mathbf{x}) \int_0^{2\pi} g(x\cos\theta + y\sin\theta, \theta)\, d\theta\, d\mathbf{x} \\
&= \int_{\mathbb{R}^2} h(\mathbf{x}) \int_0^{2\pi} \int_{-\infty}^{\infty} g(\rho, \theta)\delta(\rho - x\cos\theta - y\sin\theta)\, d\rho\, d\theta\, d\mathbf{x} \\
&= \int_0^{2\pi} \int_{-\infty}^{\infty} \int_{\mathbb{R}^2} h(\mathbf{x}) g(\rho, \theta)\delta(\rho - x\cos\theta - y\sin\theta)\, d\mathbf{x}\, d\rho\, d\theta \\
&= \int_0^{2\pi} \int_{-\infty}^{\infty} (\mathcal{R}h)(\rho, \theta) g(\rho, \theta)\, d\rho\, d\theta \\
&= \langle \mathcal{R}h, g \rangle_p, \qquad (9)
\end{aligned}$$

which confirms that $\mathcal{R}^\dagger$ is the adjoint of $\mathcal{R}$ from the inner product property of a transform and its adjoint.

Many other schemes exist for inverting the normal Radon transform. They include the "linogram" and related methods which employ a non-linear grid in the Radon domain to reduce the two-dimensional interpolation of the direct Fourier slice theorem approach to a one-dimensional interpolation in the frequency domain and a one-dimensional interpolation in the Radon domain [34]. There are also techniques that reduce the inversion of the Radon transform to a problem in linear algebra through discretization [9, 34]. Various methods exist to speed up the resulting algebra by using the special structure of the matrices involved [6, 25].

2.2 Circular Radon Transform

By analogy with (1), we define the circular Radon transform of a function to be the path integral of the function along a circle of radius t centred on the point $(u, 0)$ on the x-axis. This can be written as

$$g(u, t) = (\mathcal{R}_c f)(u, t) = \int_{-\infty}^{\infty} \int_{-\infty}^{\infty} f(x, y)\delta(t - \sqrt{(x-u)^2 + y^2})\, dx\, dy. \qquad (10)$$

The geometry of the circular Radon transform is shown in Figure 1. There are many other possible families of CRT depending on the choice of centres for the circles: the particular definition presented here has been chosen because it best corresponds to the standard geometry used in SAR.

From Papoulis [28], the Dirac delta function $\delta(\alpha(x, y))$, $\alpha(x, y) = t - \sqrt{(x-u)^2 + y^2}$ is a line mass of density

$$\frac{1}{\left(\frac{\partial \alpha}{\partial x}\right)^2 + \left(\frac{\partial \alpha}{\partial y}\right)^2} = 1.$$

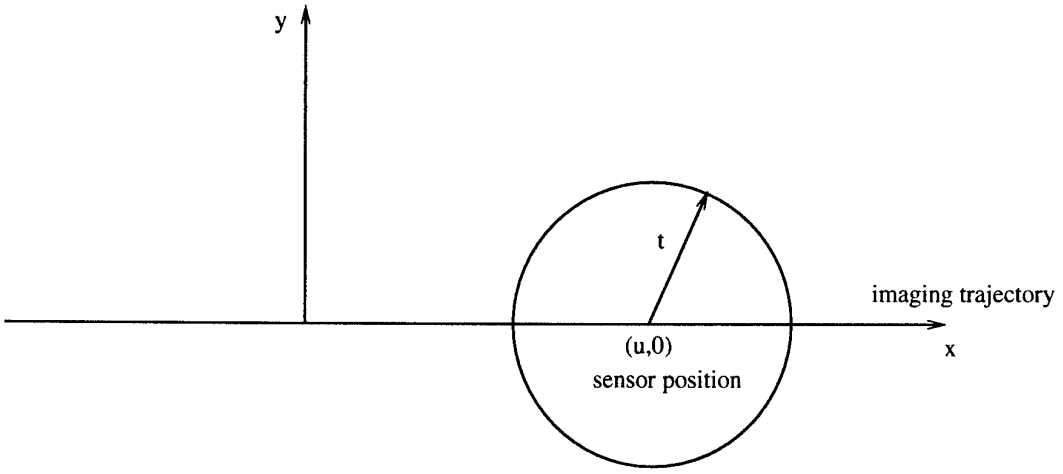

Figure 1: The geometry of the circular Radon transform.

Therefore we can rewrite (10) as

$$g(u,t) = (\mathcal{R}_c f)(u,t) = \iint_{(x-u)^2+y^2=t^2} f(x,y)\,dx\,dy. \tag{11}$$

The integral in (11) needs to be carefully interpreted as it is an integral along a line in the plane with respect to arc length. Let $x = u + t\cos\theta$ and $y = t\sin\theta$. Then from the Jacobian of the transformation of variables, $dx\,dy = t\,dt\,d\theta$. Changing the intervals of integration and eliminating the redundant integral over a single value of t we obtain as our third equivalent definition of the CRT,

$$g(u,t) = (\mathcal{R}_c f)(u,t) = \int_0^{2\pi} f(u + t\cos\theta, t\sin\theta)t\,d\theta. \tag{12}$$

From (10), the dual operator for the CRT (changing the integration with respect to x and y to be with respect to u and t), called here the *circular* backprojection operator, is defined to be

$$\begin{aligned}(\mathcal{R}_c^\dagger g)(x,y) &= \int_{-\infty}^{\infty}\int_{-\infty}^{\infty} g(u,t)\delta(t - \sqrt{(x-u)^2+y^2})\,du\,dt \\ &= \int_{-\infty}^{\infty} g(u, \sqrt{(x-u)^2+y^2})\,du. \end{aligned}\tag{13}$$

We will prove that (13) is the adjoint of the CRT in Section 2.2.1 below.

Sometimes it is convenient to define a semi-circular Radon transform (SCRT) by

$$(\mathcal{R}_{c/2} f)(u,t) = \int_0^{\pi} f(u + t\cos\theta, t\sin\theta)t\,d\theta. \tag{14}$$

2.2.1 Adjoint of the Circular Radon Transform

Given the CRT defined by (12), the dual operator defined by (13), and letting $\langle \cdot, \cdot \rangle$ and $\langle \cdot, \cdot \rangle_r$ denote inner products in $\mathbb{R}^2$ and $\mathbb{R} \times [0, \infty]$, then we can show that $\mathcal{R}_c^\dagger$ is the adjoint operator of $\mathcal{R}_c$ as follows:

$$\langle \mathcal{R}_c f, g \rangle_r = \int_{-\infty}^{\infty} \int_0^{\infty} \left(\int_0^{2\pi} f(u + t\cos\theta, t\sin\theta) t \, d\theta \right) g(u,t) \, dt \, du,$$

then setting $x = t\cos\theta$ and $y = t\sin\theta$,

$$\begin{aligned}
&= \int_{-\infty}^{\infty} \int_{-\infty}^{\infty} \int_{-\infty}^{\infty} f(x+u, y) g(u, \sqrt{x^2+y^2}) \, dx \, dy \, du \\
&= \int_{-\infty}^{\infty} \int_{-\infty}^{\infty} \int_{-\infty}^{\infty} f(x,y) g(u, \sqrt{(x-u)^2+y^2}) \, dx \, dy \, du \\
&= \int_{-\infty}^{\infty} \int_{-\infty}^{\infty} f(x,y) \left(\int_{-\infty}^{\infty} g(u, \sqrt{(x-u)^2+y^2}) \, du \right) dx \, dy \\
&= \langle f, \mathcal{R}_c^\dagger g \rangle.
\end{aligned}$$

Therefore, by the inner product property, the dual operator $\mathcal{R}_c^\dagger$ is the adjoint of $\mathcal{R}_c$.

3 Reconstruction Methods for Synthetic Aperture Radar

In this section we review simple methods for SAR image formation that allow us to establish the relationship between the received radar signal and the transformed signal or circular averages in the CRT context. We follow Soumekh [32] for the development in the first two of the following subsections, with material added to motivate the link between the radar signal and circular averages.

3.1 Time Domain Correlation

Let $p(t)$ denote the transmitted radar pulse. Then when the antenna moving along the x-axis is located at $(u, 0)$, the SAR signature of the ground point (x_i, y_i) is given by

$$p\left(t - \frac{2\sqrt{(x_i-u)^2+y_i^2}}{c} \right),$$

where c is the speed of light in the medium. Without loss of generality, we can assume that fast time t has been scaled so that it represents the distance to the point of reflectivity, effectively making $\frac{c}{2} = 1$. We will use this assumption for the remainder of this report. Therefore, the pulse becomes

$$p\left(t - \sqrt{(x_i-u)^2+y_i^2} \right).$$

In reconstruction *via* time domain correlation, this signal is correlated with the measured SAR data in the slow-time fast-time domain $s(u,t)$ to give a measure of the reflectivity at the point (x_i, y_i). Therefore we can write

$$\hat{f}(x_i, y_i) = \int_u \int_t s(u,t)\, p^\star \left(t - \sqrt{(x_i - u)^2 + y_i^2} \right) dt\, du, \tag{15}$$

where $p^\star(\cdot)$ denotes the complex conjugate of $p(\cdot)$ and $\hat{f}(x_i, y_i)$ is the estimated ground reflectivity. The integral with respect to t would normally be undertaken in the Fourier domain as an integral with respect to fast time frequency ω using Parseval's theorem,

$$\hat{f}(x_i, y_i) = \int_u \int_\omega s(u,\omega)\, P^\star(\omega) e^{2\pi i \sqrt{(x_i-u)^2+y_i^2}}\, d\omega\, du,$$

where $P(\omega)$ is the Fourier transform of the transmitted radar pulse.

How does $s(u,t)$ relate to the CRT of $f(x,y)$? This becomes clear after the following section where we show Soumekh's backprojection form of SAR image reconstruction.

3.2 Backprojection

Let s_m denote the fast-time matched filtered (*i.e.* range compressed) SAR signal given by

$$s_m(u,t) = s(u,t) * p^\star(-t). \tag{16}$$

The underlying idea of fast-time matched filtering is to try and undo the effect of convolution of the returns with the radar pulse $p(t)$. Therefore, in principle one would do this matched filtering with a function $q(t)$ whose Fourier transform $Q(\omega)$ is a reasonable approximation to $\frac{1}{P(\omega)}$. For the special case where $p(t)$ is an ideal chirp with infinite extent, then $q(t) = p^\star(-t)$. However, for other radar pulses $p^\star(-t)$ is not such a good approximation to the desired inverse filter. With the appropriate choice of $q(t)$, $s_m(u,t) = s(u,t) * q(t)$ would be close to the true unknown returns s that would have been collected by an ideal radar that emitted a delta function pulse.

Following (16), we can write

$$s_m \left(u, \sqrt{(x_i - u)^2 + y_i^2} \right) = \int_t s(u,t)\, p^\star \left(t - \sqrt{(x_i - u)^2 + y_i^2} \right) dt \tag{17}$$

and so we can rewrite the time domain correlation (15) as the backprojection

$$\hat{f}(x_i, y_i) = \int_u s_m \left(u, \sqrt{(x_i - u)^2 + y_i^2} \right) du. \tag{18}$$

Consequently, the estimated reflectivity $\hat{f}$ at the point (x_i, y_i) is given by the sum over slow-time of all the fast-time points that correspond to echoes from that point. This corresponds to integrating along a hyperbolic path in the transform or slow-time fast-time domain, because for fixed (x_i, y_i), the function $t = \sqrt{(x_i - u)^2 + y_i^2}$ describes a (conjugate) hyperbola centred on $(x_i, 0)$ in the (u,t) plane (concave upwards) with asymptotes of slope ± 1.

3.3 Link to the Circular Radon Transform

The linkage between the circular Radon transform and reconstruction *via* backprojection and hence time domain correlation of the previous subsections can now be explained. We can write the received radar signal as the integral over the product of the combined antenna pattern, gain, range attenuation, and reflectivity function with the pulse to give [38],

$$s(u,t) = \int_y \int_x A(u,x,y) f(x,y)\, p\left(t - \sqrt{(x-u)^2 + y^2}\right)\, dx\, dy,$$

where $A(u,x,y)$ is the combined antenna pattern, gain and range attenuation function, and $f(x,y)$ is the reflectivity function. Next we assume that the reflectivity function is non-zero only in the main antenna beam so that the frequency-independent antenuation function is unity, giving

$$s(u,t) = \int_y \int_x f(x,y)\, p\left(t - \sqrt{(x-u)^2 + y^2}\right)\, dx\, dy. \tag{19}$$

Then substituting (19) into (17) and letting $t' = \sqrt{(x-u)^2 + y^2}$ and $t'' = \sqrt{(x'-u)^2 + y'^2}$ we obtain

$$\begin{aligned} s_m(u,t') &= \int_t \left[\int_{y'} \int_{x'} f(x',y')\, p\left(t - t''\right)\, dx'\, dy' \right] p^\star\left(t - t'\right)\, dt \\ &= \int_{y'} \int_{x'} f(x',y') h(u,t',t'')\, dx'\, dy' \end{aligned} \tag{20}$$

where $h(u,t',t'')$ is given by

$$h(u,t',t'') = \int_t p\left(t - t''\right)\, p^\star\left(t - t'\right)\, dt$$

and can be considered to be the point spread function of the radar. For a chirp pulse $h(u,t',t'')$ is concentrated at t'.

We can now make the following observations. Firstly, at the radar sampling points (x,y), the point spread function $h(u,t',t'')$ and the delta function $\delta(t - \sqrt{(x-u)^2 + y^2})$ will coincide, so from (20) and (13) the fast-time matched filtered SAR signal $s_m(u,t)$ is the function $g(u,t)$ of circular averages, or circular Radon transformed data, to the limit of the radar resolution. Secondly, the backprojection (18) is identical to the circular backprojection (13). Thirdly, $\hat{f}(x,y)$ is not the target or ground reflectivity function $f(x,y)$ because the adjoint $\mathcal{R}_c^\dagger$ is not equal to the inverse $\mathcal{R}_c^{-1}$, although it can be a reasonable approximation to it in situations where the scatterers are isolated points such as in sonar.

4 The Problem

The SAR image reconstruction problem, given the data $g(u,t)$ consisting of integrals of $f(x,y)$ over circular arcs in the plane centred on the x axis, is to find a closed form

solution for f. In SAR terms, g represents the range-compressed baseband received signal in fast-time t and slow-time u coordinates as discussed in the previous section. As in (11), we may write the relationship between f and g as

$$g(u,t) = (\mathcal{R}_c f)(u,t) = \iint_{(x-u)^2+y^2=t^2} f(x,y)\,dx\,dy. \tag{21}$$

The geometry is shown in Figure 1.

We shall interpret (21) here as the equivalent form shown in (12),

$$g(u,t) = \int_0^{2\pi} f(u + t\cos\theta, t\sin\theta)t\,d\theta. \tag{22}$$

When g is data collected from a SAR system, then (22) should more properly be [14],

$$g(u,t) = \int_0^{2\pi} h(t)\mu(\theta)f(u + t\cos\theta, t\sin\theta)t\,d\theta, \tag{23}$$

where $h(t)$ is the range attenuation factor under the omnidirectional isotropic scattering model, and $\mu(\theta)$ represents the antenna diagram assuming no frequency dependence. We will assume that the range attenuation factor has been compensated for in the processing to form $g(u,t)$ and so can be neglected here. We will also assume that the target is in the main beam so that the antenna diagram can also be neglected.

We may assume that $f(x,y) = 0$ for $y < 0$ or that $f(x,y) = f(x,-y)$ as convenient because either the SAR points to one side of the platform or for low frequency SAR, two antennas are to used to distinguish the left- and right-hand sides [15]. Note here that the CRT annihilates functions $f(x,y)$ that are odd in y (*i.e.* $f(x,y) = -f(x,-y)$), and this property has important consequences. In particular, the inversion formulae typically give reconstructions f that are even, so if we know $f(x,y) = 0$ for $y < 0$, we will need to multiply reconstructions by a factor of two to give the correct answer in the upper half plane. Furthermore, many of the changes of variables to be considered shortly involve square roots, and so implicitly restrict domains of definition or make the function symmetric.

4.1 Invertibility of the Circular Radon Transform

The Radon transform integrating over all circles in the plane $\mathbb{R}^2$ is clearly overdetermined, because the set of all circles has three dimensions, which is one greater than the plane. The question then is what subsets of circles in the plane are invertible. Quinto [30] considers the case of all translations of a circle of fixed radius as well as all circles centred on a circle and shows they are invertible. Agranovsky and Quinto [1] show that the more general case of CRTs along paths that are not on the zero sets of harmonic polynomials are invertible. The CRT along the lines considered in this report is a special case. Zalcman [39] provides an excellent introduction to these sorts of considerations in integral geometry.

5 Previous Methods for Inverting the Circular Radon Transform

5.1 Hankel Transform Method

The inverse of the CRT can be expressed analytically in terms of a Hankel transform as follows. This was discovered independently by Fawcett [12] and Andersson [2], and rediscovered more recently by Soumekh [31] and Milman [21, 22] as a statement of the ω-k migration (or range migration) algorithm [8]. We will firstly derive the inverse in terms of the Hankel transform as presented by Nilsson in [26].

Firstly, define the CRT by

$$g(u,t) = (\mathcal{R}_c f)(u,t) = \int_0^{2\pi} f(u + t\cos\theta, t\sin\theta)\, d\theta. \tag{24}$$

Note that in (24), the term t has been neglected from the definition (12). It is simply a scaling of the radar signal $g(u,t)$ so it is possible to neglect it here without loss of generality. Next, take the Fourier transform with respect to slow time u,

$$\begin{aligned} g^{(F,I)}(v,t) &= \int_{-\infty}^{\infty} e^{2\pi i v u} g(u,t)\, du \\ &= \int_{-\infty}^{\infty} e^{2\pi i v u} \left(\int_0^{2\pi} f(u + t\cos\theta, t\sin\theta)\, d\theta \right) du \end{aligned}$$

where $g^{(F,I)}$ denotes the Fourier transform with respect to the first variable and the second variable is left intact. Changing the order of integration,

$$\begin{aligned} g^{(F,I)}(v,t) &= \int_{-\infty}^{\infty} \int_0^{2\pi} e^{2\pi i v(u+t\cos\theta)} e^{-2\pi i v t\cos\theta} f(u + t\cos\theta, t\sin\theta)\, d\theta\, du \\ &= \int_0^{2\pi} e^{-2\pi i v t\cos\theta} \int_{-\infty}^{\infty} e^{2\pi i v(u+t\cos\theta)} f(u + t\cos\theta, t\sin\theta)\, du\, d\theta \\ &= \int_0^{2\pi} e^{-2\pi i v t\cos\theta} f^{(F,I)}(v, t\sin\theta)\, d\theta. \end{aligned}$$

Now,

$$f^{(F,I)}(v,y) = \int_{-\infty}^{\infty} f^{(F,F)}(v,\rho) e^{-2\pi i \rho y}\, d\rho$$

where $y = t\sin\theta$. Then changing the order of integration,

$$\begin{aligned} g^{(F,I)}(v,t) &= \int_0^{2\pi} e^{-2\pi i v t\cos\theta} \left(\int_{-\infty}^{\infty} f^{(F,F)}(v,\rho) e^{-2\pi i \rho y}\, d\rho \right) d\theta \\ &= \int_{-\infty}^{\infty} f^{(F,F)}(v,\rho)\, d\rho \int_0^{2\pi} e^{-2\pi i t(v\cos\theta + \rho\sin\theta)}\, d\theta. \end{aligned}$$

Let

$$v\cos\theta + \rho\sin\theta = \sqrt{v^2+\rho^2}\sin(\theta - \psi)$$

for some ψ. Therefore using periodicity of the integrand,

$$\int_0^{2\pi} e^{-2\pi i t\sqrt{v^2+\rho^2}\sin(\theta-\psi)}\,d\theta = \int_0^{2\pi} e^{-2\pi i t\sqrt{v^2+\rho^2}\sin\theta}\,d\theta$$
$$= 2\pi J_0(2\pi t\sqrt{v^2+\rho^2})$$

where $J_0(\cdot)$ is the Bessel function of the first kind of order zero. Consequently,

$$g^{(F,I)}(v,t) = 2\pi\int_{-\infty}^{\infty} f^{(F,F)}(v,\rho)J_0(2\pi t\sqrt{v^2+\rho^2})\,d\rho.$$

Next, let

$$\sigma = \sqrt{v^2+\rho^2} \tag{25}$$

so that

$$d\rho = \frac{\sigma\,d\sigma}{\sqrt{\sigma^2-v^2}}$$

and so then

$$g^{(F,I)}(v,t) = 2\pi\int_{-\infty}^{\infty} J_0(2\pi t\sigma)\frac{f^{(F,F)}(v,\sqrt{\sigma^2-v^2})}{\sqrt{\sigma^2-v^2}}\sigma\,d\sigma. \tag{26}$$

We can use the symmetry in the problem to reduce the interval of integration in (26). From $f(x,-y) = f(x,y)$, we have $f^{(F,F)}(v,-\rho) = f^{(F,F)}(v,\rho)$ and from (25) we have $\sigma = \sqrt{v^2} = |v|$ when $\rho = 0$. Therefore,

$$g^{(F,I)}(v,t) = 4\pi\int_{|v|}^{\infty} J_0(2\pi t\sigma)\frac{f^{(F,F)}(v,\sqrt{\sigma^2-v^2})}{\sqrt{\sigma^2-v^2}}\sigma\,d\sigma.$$

Then from the Hankel transform pair of order zero [5],

$$f^{H_0}(q) = 2\pi\int_0^{\infty} f(r)J_0(2\pi qr)r\,dr$$
$$f(r) = 2\pi\int_0^{\infty} f^{H_0}(q)J_0(2\pi qr)q\,dq$$

we have that

$$g^{(F,H_0)}(v,\sigma) = \begin{cases} 2\frac{f^{(F,F)}(v,\sqrt{\sigma^2-v^2})}{\sqrt{\sigma^2-v^2}} & \text{if } \sigma-|v|\geqslant 0 \\ 0 & \text{otherwise.}\end{cases}$$

Let

$$|\rho| = \sqrt{\sigma^2-v^2},$$

then

$$f^{(F,F)}(v,\rho) = \frac{|\rho|}{2}g^{(F,H_0)}(v,\sqrt{\rho^2+v^2}) \tag{27}$$

where $g^{(F,H_0)}$ is the Fourier transform of g with respect to the first variable u and zero-order Hankel transform with respect to the second variable t of $g(u,t)$, given by,

$$g^{(F,H_0)}(v,\rho) = 2\pi\int_{-\infty}^{\infty}\int_0^{\infty} g(u,t)e^{2\pi ivu}J_0(2\pi t\rho)t\,dt\,du.$$

Note that $f^{(F,F)}(v,\rho)$ is implicitly even in ρ.

5.2 Backprojection Method

Andersson [2] showed that the backprojection operator for the CRT (the adjoint expressed in (13)) can be used to implement $g^{(F,H_0)}$ in (27). We give the following development from Nilsson [26].

Again we take the backprojection operator to be

$$(\mathcal{R}_c^\dagger g)(x,y) = \int_{-\infty}^{\infty} g(u, \sqrt{(x-u)^2+y^2})\, du \tag{28}$$

then taking the two-dimensional Fourier transform of $\mathcal{R}_c^\dagger g$ we obtain

$$\begin{aligned}
(\mathcal{R}_c^\dagger g)^{(F,F)}(v,\rho) &= \int_{-\infty}^{\infty}\int_{-\infty}^{\infty}\left(\int_{-\infty}^{\infty} g(u, \sqrt{(x-u)^2+y^2})\, du\right) e^{2\pi i(vx+\rho y)}\, dx\, dy \\
&= \int_{-\infty}^{\infty} e^{2\pi iuv}\left(\int_{-\infty}^{\infty}\int_{-\infty}^{\infty} g(u, \sqrt{(x-u)^2+y^2}) e^{2\pi i\rho y} e^{2\pi iv(x-u)}\, dx\, dy\right) du \\
&= \int_{-\infty}^{\infty} e^{2\pi iuv}\left(\int_{-\infty}^{\infty}\int_{-\infty}^{\infty} g(u, \sqrt{x^2+y^2}) e^{2\pi i\rho y} e^{2\pi ivx}\, dx\, dy\right) du,
\end{aligned}$$

and letting $x = t\cos\theta$, $y = t\sin\theta$,

$$\begin{aligned}
&= \int_{-\infty}^{\infty} e^{2\pi iuv}\left(\int_0^{\infty}\int_0^{2\pi} g(u,t) e^{2\pi it(v\cos\theta+\rho\sin\theta)} t\, dt\, d\theta\right) du \\
&= \int_{-\infty}^{\infty}\int_0^{\infty} g(u,t) e^{2\pi iuv}\left(\int_0^{2\pi} e^{2\pi it\sqrt{v^2+\rho^2}\sin(\theta-\psi)}\, d\theta\right) t\, dt\, du \\
&= \int_{-\infty}^{\infty}\int_0^{\infty} g(u,t) J_0(2\pi t\sqrt{v^2+\rho^2}) e^{2\pi iuv} t\, dt\, du \\
&= \frac{1}{2\pi} g^{(F,H_0)}(v, \sqrt{v^2+\rho^2}).
\end{aligned} \tag{29}$$

Therefore, from (27) and (29),

$$f^{(F,F)}(v,\rho) = \pi|\rho|(\mathcal{R}_c^\dagger g)^{(F,F)}(v,\rho). \tag{30}$$

5.3 Fast Backprojection Method

Nilsson [26] has developed a fast backprojection method for the operator (28). This is similar to the method developed in [20]. Nilsson's method has been applied to the CARABAS-II low-frequency ultra-wideband VHF SAR sensor [35, 36].

5.4 Link to the Range Migration Algorithm

Milman [22] has shown that the range migration algorithm (RMA) [8, 21, 31] can be viewed as a close approximation to a Hankel-Fourier transform representation of the inverse CRT, similar to the one presented in Section 5.1. We will now examine this development in detail.

Starting with the CRT[1],

$$g(u,t) = \iint_{(x-u)^2+y^2=t^2} f(x,y)\,dx\,dy,$$

Milman noted that the hyperbolic geometry in the (u,t)-plane suggests the use of hyperbolic functions to simplify the integrals. Re-arranging the circle of integration,

$$-\frac{(u-x)^2}{y^2} + \frac{t^2}{y^2} = 1,$$

we see that it defines a rectangular conjugate hyperbola in the (u,t)-plane centred on $(x,0)$, with parametric representation $(y\sinh\psi + x, y\cosh\psi)$, $\psi \in \mathbb{R}$. Therefore, if we define

$$y\sinh\psi = x - u$$

then using the identity $\cosh^2\psi - \sinh^2\psi = 1$ we obtain

$$\begin{aligned} x &= t\tanh\psi + u \\ y &= t\,\mathrm{sech}\,\psi. \end{aligned}$$

The Jacobian of the transformation $(x,y) \longrightarrow (t,\psi)$ is $-t\,\mathrm{sech}\,\psi$ so $dx\,dy = t\,\mathrm{sech}\,\psi\,d\psi$, and we can write

$$g(u,t) = \int_{-\infty}^{\infty} f(t\tanh\psi + u, t\,\mathrm{sech}\,\psi)t\,\mathrm{sech}\,\psi\,d\psi.$$

Let

$$g_0(u,t) = \frac{g(u,t)}{t}.$$

Then taking the two-dimensional Fourier Transform of $g_0(u,t)$ we have

$$g_0^{(F,F)}(v,k) = \int_{-\infty}^{\infty}\int_{-\infty}^{\infty}\int_{-\infty}^{\infty} e^{2\pi i(vu+kt)} f(t\tanh\psi + u, t\,\mathrm{sech}\,\psi)\,\mathrm{sech}\,\psi\,d\psi\,du\,dt,$$

and letting $t = y\cosh\psi$ so that $dy = dt\,\mathrm{sech}\,\psi$,

$$= \int_{-\infty}^{\infty}\int_{-\infty}^{\infty}\int_{-\infty}^{\infty} e^{2\pi i(vu+ky\cosh\psi)} f(y\sinh\psi + u, y)\,d\psi\,du\,dy$$

and letting $u = x - y\sinh\psi$ so that $du = dx$,

$$= \int_{-\infty}^{\infty}\int_{-\infty}^{\infty}\int_{-\infty}^{\infty} e^{2\pi i(ky\cosh\psi - vy\sinh\psi)} e^{2\pi ivx} f(x,y)\,d\psi\,dx\,dy. \tag{31}$$

[1]Milman included an $e^{4\pi i\frac{t}{\lambda}}$ term in his definition, where λ is the wavelength of the radiation. We do not need this term because we assume that the differing phase lags with respect to frequency have already been taken into account by the radar to measure $p\left(t - \frac{2\sqrt{(x_i-u)^2+y_i^2}}{c}\right)$.

Next, we let $k_y^2 = k^2 - v^2$ (this is called the *Stolt* transformation [8]). Also we define

$$\cosh\phi = \frac{k}{k_y}, \qquad \sinh\phi = \frac{v}{k_y}, \qquad \phi \in \mathbb{R},$$

and we can see as expected that

$$\cosh^2\phi - \sinh^2\phi = \frac{k^2 - v^2}{k_y^2} = 1.$$

Then,

$$\begin{aligned}\cosh(\psi - \phi) &= \cosh\psi\cosh\phi - \sinh\psi\sinh\phi \\ &= \frac{k}{k_y}\cosh\psi - \frac{v}{k_y}\sinh\psi,\end{aligned}$$

and we can rewrite (31) as

$$g_0^{(F,F)}(v,k_y) = \int_{-\infty}^{\infty}\int_{-\infty}^{\infty}\int_{-\infty}^{\infty} e^{2\pi i v x} e^{2\pi i y k_y \cosh(\psi-\phi)} f(x,y)\,d\psi\,dx\,dy \tag{32}$$

The Hankel functions of the first and second kind (also called Bessel functions of the third kind) are given by the integral representations [19]

$$\begin{aligned}H_0^{(1)}(x) &= \frac{1}{\pi i}\int_{-\infty}^{\infty} e^{ix\cosh t}\,dt \\ H_0^{(2)}(x) &= -\frac{1}{\pi i}\int_{-\infty}^{\infty} e^{-ix\cosh t}\,dt.\end{aligned}$$

So we can rewrite (32) as

$$g_0^{(F,F)}(v,k_y) = \int_{-\infty}^{\infty}\int_{-\infty}^{\infty} H_0^{(1)}(2\pi y k_y) e^{2\pi i v x} f(x,y)\,dx\,dy, \tag{33}$$

after ignoring the ϕ term because we are integrating over an infinite domain. Using the Hankel functions as a kernel, the Hankel transform pair of order zero is here defined to be

$$\begin{aligned}f^{(H_0')}(q) &= 2\pi\int_{-\infty}^{\infty} H_0^{(1)}(2\pi q r) f(r) r\,dr \\ f(r) &= 2\pi\int_{-\infty}^{\infty} H_0^{(2)}(2\pi q r) f^{(H_0')}(q) q\,dq.\end{aligned}$$

Let $f_0(x,y) = f(x,y)/y$. Then (33) can be rewritten as

$$g_0^{(F,F)}(v,k_y) = \frac{1}{2\pi} f_0^{(F,H_0')}(v,k_y), \tag{34}$$

or in other words, the two-dimensional Fourier transform of g_0 (after the Stolt transformation) is equal to the Fourier transform with respect to x and the Hankel transform of order zero with respect to y of $f_0(x,y)$. Therefore, we can write that

$$\frac{f(x,y)}{y} = \int_{-\infty}^{\infty}\int_{-\infty}^{\infty} e^{-2\pi i v x} H_0^{(2)}(2\pi y k_y) g_0^{(F,F)}(v,k_y) k_y\,dk_y\,dv. \tag{35}$$

The asymptotic expansion of $H_0^{(2)}(z)$ for large z is given by [17],

$$H_0^{(2)}(z) \approx \sqrt{\frac{2}{\pi z}} e^{-i(z-\frac{\pi}{4})} \sum_{n=0}^{\infty} \frac{\Gamma\left(n+\frac{1}{2}\right)\left(-\frac{i}{2z}\right)^n}{n!\,\Gamma\left(-n+\frac{1}{2}\right)}, \tag{36}$$

and taking only the first term of the expansion we obtain

$$H_0^{(2)}(z) \approx \sqrt{\frac{2}{\pi z}} e^{-i(z-\frac{\pi}{4})}. \tag{37}$$

(Note that this is equivalent to making the stationary phase approximation [22].) Therefore we can rewrite (35) as

$$f(x,y) \approx \frac{1+i}{\pi\sqrt{2}} \sqrt{y} \int_{-\infty}^{\infty} \int_{-\infty}^{\infty} e^{-2\pi i(vx+k_y y)} \sqrt{k_y}\, g_0^{(F,F)}(v,k_y)\, dk_y\, dv. \tag{38}$$

5.4.1 Shift to Scene Centre

The origin of the swath is usually shifted from the antenna position to the centre of the swath to reduce the bandwidth of a signal. To achieve this let the centre of the swath be (x_0, y_0), and define the new coordinates $x' = x - x_0$ and $y' = y - y_0$. Then we rewrite (32) as[2]

$$g_0^{(F,F)}(v,k_y) = e^{2\pi i v x_0} \int_{-\infty}^{\infty} \int_{-\infty}^{\infty} \int_{-\infty}^{\infty} e^{2\pi i v x'} e^{2\pi i (y'+y_0) k_y \cosh(\psi-\phi)} f'(x',y')\, d\psi\, dx'\, dy', \tag{39}$$

where $f'(x',y') = f(x'+x_0, y'+x_0)$. Then following through the steps of the previous subsection, we obtain

$$f'(x',y') \approx \frac{1+i}{\pi\sqrt{2}} \frac{y'}{\sqrt{y'+y}} \int_{-\infty}^{\infty} \int_{-\infty}^{\infty} e^{-2\pi i(vx'+k_y y')} \sqrt{k_y}\, e^{-2\pi i v x_0} e^{-2\pi i k_y y_0}\, g_0^{(F,F)}(v,k_y)\, dk_y\, dv. \tag{40}$$

5.4.2 Statement of the Range Migration Algorithm

We are now in a position to state the RMA from (40):

1. Compute the two-dimensional Fourier transform of the scaled signal $g_0(u,t)$ to obtain $g_0^{(F,F)}(v,k)$.
2. "Match filter": compute $\sqrt{k_y}\, e^{-2\pi i v x_0} e^{-2\pi i k_y y_0}\, g_0^{(F,F)}(v,k)$.
3. Perform the Stolt transform $k_y^2 = k^2 - v^2$ by interpolation and resampling of the second variable k to obtain $\sqrt{k_y}\, e^{-2\pi i v x_0} e^{-2\pi i k_y y_0}\, g_0^{(F,F)}(v,k_y)$.
4. Compute the scaled inverse two-dimensional Fourier transform (40) of the output of the previous step to obtain $f'(x',y')$.

Consequently, we can see that the RMA is an approximation to a Hankel-Fourier transform formulation of the inverse CRT.

[2]Note the difference from (27) of [22]. The presence of the $\cosh(\psi-\phi)$ term means that it is incorrect to take an $e^{2\pi i k_y y}$ term outside the integrals.

5.4.3 Validity of the Hankel Function Approximation

How accurate is the approximation in (37)? This will determine whether the novel techniques we develop later in this report have practical utility, because the range migration algorithm is a widely understood public domain algorithm, which is believed to cope completely with range migration and be applicable to high squint and ultra-wideband SAR [8].

From Lebedev [19], the residual of the approximation in (36) is given by

$$|r_n(z)| \leqslant \frac{\Gamma^2(n+\frac{2}{3})\sqrt{2|z|}}{\pi\, n!(2|z|\sin\delta)^{n+\frac{3}{2}}}, \qquad |\arg z| \leqslant \pi - \delta,$$

where δ is an arbitrarily small positive number. When $n = 0$ (taking the first term in the expansion (36)), $r_n(z)$ simplifies to

$$|r_n(z)| \leqslant \frac{1}{8|z|(\sin\delta)^{\frac{3}{2}}} = \mathcal{O}\left(\frac{1}{|z|}\right). \tag{41}$$

Therefore, the error in the approximation (37) is of the order of $1/(yk_y)$, but the constant factor could be extremely large due to the presence of the $(\sin\delta)^{\frac{3}{2}}$ in (41).

Figure 2 shows the magnitude of the residual

$$r_0(z) = H_0^{(2)}(z) - \sqrt{\frac{2}{\pi z}}e^{-i(z-\frac{\pi}{4})}, \tag{42}$$

where for our purposes $z = 2\pi y k_y$ from (35). Clearly the residual decays to zero rapidly as expected from (41). We will now examine the range of values of $z = 2\pi y k_y$ that are likely to be encountered in practice.

The signal support of the range spatial frequencies k_y is determined from the fast-time and slow-time spatial frequencies k and v, respectively, by $k_y^2 = k^2 - v^2$. The fast-time spatial frequency k has units of radians/m and signal support given by [8]

$$k \in [4\pi(f_c - B/2)/c, 4\pi(f_c + B/2)/c],$$

where f_c is the radar centre frequency (Hz) and B is its transmitted bandwidth (Hz). For the n-th target, its slow-time spatial frequency v has support [32]

$$v \in \Omega_n = [2\frac{\omega}{c}\cos\theta_n(-L), 2\frac{\omega}{c}\cos\theta_n(L)],$$

where $\theta_n(u)$ is the aspect angle (measured off trajectory) of the n-th target when the radar is located at $(u, 0)$, L is half the size of the synthetic aperture, and $\omega = 2\pi f$ is the transmitted signal's instantaneous angular velocity (radians/s). For a given fast-time frequency k, the slow-time spatial frequency signal support of v for the total echoed SAR signal $s(u,t)$, denoted Ω_s, is given by the union of that for all targets in the target area. For spotlight mode and a planar radar aperture, [32]

$$\Omega_s \approx \left[2\frac{\omega}{c}\cos\theta_c - 2\frac{\omega}{c}\left(\frac{L\sin^2\theta_c}{x_c} + \frac{\lambda}{D_x}\right), 2\frac{\omega}{c}\cos\theta_c + 2\frac{\omega}{c}\left(\frac{L\sin^2\theta_c}{x_c} + \frac{\lambda}{D_x}\right)\right],$$

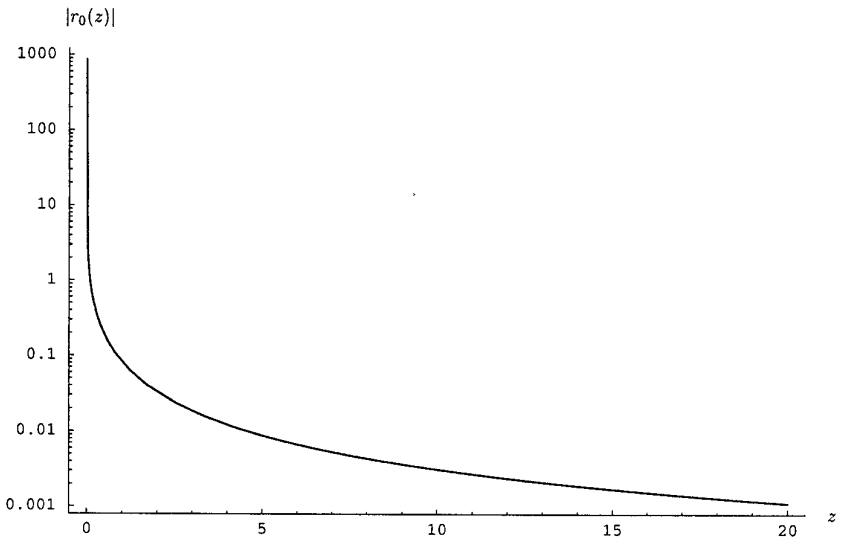

Figure 2: The magnitude of the residual: $r_0(z)$.

where θ_c is the average squint angle (measured off trajectory), x_c is the mean range of the target area, D_x is the length of the antenna, and $\lambda = 2\pi c/\omega$ is the instantaneous wavelength of the radiation.

Using the above equations for the support of fast-time and slow-time spatial frequencies, it is possible to show when problems are likely to occur with the RMA. In surveillance and mapping applications, the standoff to the swath is usually measured in kilometers. If we take the example given in Table 10.1, p. 410 of [8], the minimum slant range of the imaged scene is $y = 712.35$ m for a radar with a radar centre frequency of 242.2 MHz. The transmitted bandwidth is $B = 133.5$ MHz, the half synthetic aperture $L = 380.4$ m, and we assume that the antenna length $D_x = 4$ m for a broadside geometry. Then $k \in [7.3576, 12.9496]$ radians/m, and $v \in \Omega_s \approx [-5.94043, 5.94043]$ at the minimum instantaneous frequency. Therefore $z = 2\pi y\sqrt{k^2 - v^2} = 19430.3$ in this example. However, by shortening the antenna length D_x it is possible to make k_y arbitrarily close to zero which puts one in the regime where the approximation residual is large. Further investigation is required to understand when this is likely to occur in practical systems, but this simple example shows that it is possible in practice.

5.5 Deconvolution Method

Norton [27] in the context of acoustic imaging has developed a method to reconstruct a reflectivity field from line integrals over circular paths. Following [27], we may rewrite (21) in terms of Dirac delta functions so that

$$g(u,t) = \int_{-\infty}^{\infty}\int_{-\infty}^{\infty} f(x,y)\,\delta\left(t - \sqrt{(x-u)^2 + y^2}\right)\,dx\,dy. \tag{43}$$

Norton then uses the property of the Dirac delta function that

$$\delta(z-a) = 2z\,\delta(z^2-a^2) \tag{44}$$

for $x > 0$ and $a > 0$ to write

$$g(u,t) = 2t\int_{-\infty}^{\infty}\int_{-\infty}^{\infty} f(x,y)\,\delta\left(t^2-(x-u)^2-y^2\right)\,dx\,dy. \tag{45}$$

This manipulation is not correct, however, because the substitution of (44) into (43) has used $z = t$ and $a = \sqrt{(x-u)^2+y^2}$, which is only appropriate if the integral (43) is with respect to t, but it isn't. Consequently, the equations Norton derives to invert (45) are not the inverse of (43).

6 Resampled Fourier Methods for Inverting the Circular Radon Transform

We now present a novel method for inverting the circular Radon transform *via* Fourier transforms and appropriate resamplings. We derive the result by two different methods and show that they are equivalent; firstly directly *via* change of variables, and secondly *via* the projection slice theorem.

6.1 Square Fourier Transform Method

Firstly, let us define the square Fourier transform (FT) of the received signal g by

$$G(u,\omega) = \int_{-\infty}^{\infty} e^{2\pi i\omega t^2} g(u,t)\,dt, \tag{46}$$

then from (22)

$$G(u,\omega) = \int_{-\infty}^{\infty}\int_{0}^{2\pi} e^{2\pi i\omega t^2} f(u+t\cos\theta, t\sin\theta)t\,dt\,d\theta.$$

Making the change of coordinates from polar (t,θ) to Cartesian (x,y) ($dx\,dy = t\,dt\,d\theta$ from the Jacobian) and then translating in x so that $(u,0)$ is now the origin gives

$$\begin{aligned} G(u,\omega) &= 2\int_{-\infty}^{\infty}\int_{-\infty}^{\infty} e^{2\pi i\omega((x-u)^2+y^2)} f(x,y)\,dx\,dy \\ &= 2e^{2\pi i\omega u^2}\int_{-\infty}^{\infty}\int_{-\infty}^{\infty} e^{2\pi i\omega(x^2+y^2)} e^{-2\pi i(-2\omega u)x} f(x,y)\,dx\,dy. \end{aligned} \tag{47}$$

Next, make the change of variable $r = x^2+y^2$ so that

$$\begin{aligned} x &= x \\ y &= \sqrt{r-x^2}. \end{aligned} \tag{48}$$

The Jacobian of this transformation is

$$J = \frac{\partial(x,y)}{\partial(x,r)} = \begin{vmatrix} \frac{\partial x}{\partial x} & \frac{\partial x}{\partial r} \\ \frac{\partial y}{\partial x} & \frac{\partial y}{\partial r} \end{vmatrix} = \begin{vmatrix} 1 & 0 \\ \frac{-x}{\sqrt{r-x^2}} & \frac{1}{2\sqrt{r-x^2}} \end{vmatrix} = \frac{1}{2\sqrt{r-x^2}}$$

so then

$$dx\,dy = \frac{1}{2\sqrt{r-x^2}}\,dx\,dr.$$

We define the function $k(x,r)$ by

$$k(x,r) = \begin{cases} \frac{f(x,\sqrt{r-x^2})}{\sqrt{r-x^2}} & 0 < |x|^2 < r \\ 0 & \text{otherwise,} \end{cases} \tag{49}$$

where we have assumed that $f(x,y) = f(x,-y)$ so we need only consider the positive root of $\sqrt{r-x^2}$.

Then we can rewrite $G(u,\omega)$ in (47) as

$$\begin{aligned} G(u,\omega) &= 2e^{2\pi i\omega u^2} \int_{-\infty}^{\infty}\int_{-\infty}^{\infty} e^{2\pi i\omega r} e^{2\pi i(-2\omega u)x} \frac{f(x,\sqrt{r-x^2})}{2\sqrt{r-x^2}}\,dx\,dr \\ &= e^{2\pi i\omega u^2} \int_{-\infty}^{\infty}\int_{-\infty}^{\infty} e^{2\pi i(-2\omega u)x} e^{2\pi i\omega r} k(x,r)\,dx\,dr \\ &= e^{2\pi i\omega u^2} K(-2\omega u,\omega) \end{aligned} \tag{50}$$

where

$$\begin{aligned} K(\alpha,\beta) &= \int_{-\infty}^{\infty}\int_{-\infty}^{\infty} e^{2\pi i\alpha x} e^{2\pi i\beta r} k(x,r)\,dx\,dr \\ &= e^{-\pi i\frac{\alpha^2}{2\beta}} G(-\frac{\alpha}{2\beta},\beta). \end{aligned} \tag{51}$$

Calculating the Inverse

Consequently, given $g(u,t)$, the inversion of the CRT can be carried out by the following series of resamplings and Fourier transforms. Firstly, let $h(u,\tau)$ be a scaled resampling of $g(u,t)$ defined by

$$h(u,\tau) = \frac{g(u,\sqrt{\tau})}{2\sqrt{\tau}}. \tag{52}$$

This resampling converts the square FT of g in (46) into the standard FT of h, so that

$$G(u,\omega) = \int_{-\infty}^{\infty} e^{2\pi i\omega\tau} h(u,\tau)\,d\tau. \tag{53}$$

Next, we resample G according to

$$K(\alpha,\beta) = e^{-\pi i\frac{\alpha^2}{2\beta}} G(-\frac{\alpha}{2\beta},\beta) \tag{54}$$

and then compute $k(x,r)$ by the two-dimensional FT of K by

$$k(x,r) = \int_{-\infty}^{\infty}\int_{-\infty}^{\infty} e^{-2\pi i\alpha x}e^{-2\pi i\beta r}K(\alpha,\beta)\,d\alpha\,d\beta \tag{55}$$

which we resample to give $f(x,y)$ by

$$f(x,y) = y\,k(x,x^2+y^2). \tag{56}$$

Note that we have used this method to compute some analytic inverse CRTs in Section 7.3.

6.2 Reduction to a Normal Radon Transform

Starting with (22) we make the change of variable $x = u + t\cos\theta$ so that

$$dx = -t\sin\theta\,d\theta$$
$$\sin\theta = \sqrt{1-\frac{(x-u)^2}{t^2}},$$

and using $f(x,y) = f(x,-y)$, we can rewrite the integral in x as

$$g(u,t) = -2\int_{u+t}^{u-t} f(x,\sqrt{t^2-(x-u)^2})\frac{t}{\sqrt{t^2-(x-u)^2}}\,dx.$$

Now $y = \sqrt{t^2-(x-u)^2}$, and making the change of variables $(x,y) \longleftrightarrow (x,r)$ as in (48), *i.e.* $r = x^2+y^2$, we have that $\sqrt{r-x^2} = \sqrt{t^2-(x-u)^2}$ and $r = t^2-u^2+2xu$. Therefore, from the definition of $k(x,r)$ in (49), we obtain that

$$g(u,t) = \int_{u-t}^{u+t} 2k(x,t^2-u^2+2xu)t\,dx. \tag{57}$$

We recognise this as the integral along the straight line $x\cos\theta + r\sin\theta = \rho$ in the (x,r) plane where

$$\cos\theta = -\frac{2u}{\sqrt{1+4u^2}}, \qquad \sin\theta = \frac{1}{\sqrt{1+4u^2}}, \qquad \rho = \frac{t^2-u^2}{\sqrt{1+4u^2}}. \tag{58}$$

However, the integral is not with respect to arc length along the line: to achieve this we note that

$$dl = \sqrt{1+4u^2}\,dx, \tag{59}$$

which takes into account the length of the line, so that the normal Radon transform $(\mathcal{R}k)(\rho,\theta)$ of $k(x,r)$ is given by

$$\begin{aligned}(\mathcal{R}k)(\rho,\theta) &= \int_{(x,r):\,x\cos\theta+r\sin\theta=\rho} k(x,r)\,dl \\ &= \sqrt{1+4u^2}\int_{-\infty}^{\infty} k(x,t^2-u^2+2xu)\,dx.\end{aligned} \tag{60}$$

We can extend the limits of integration of (57) to $(-\infty, \infty)$ by noting that $k(x,r) = 0$ for $|x| > r$, $r \leqslant 0$. Therefore, we can rewrite (60) as

$$(\mathcal{R}k)(\rho,\theta) = \frac{\sqrt{1+4u^2}}{2t} g(u,t). \tag{61}$$

Nilsson [26] has developed a very similar expression to this to relate the CRT to backprojection along straight lines.

By appealing to the projection slice theorem, we can write

$$\begin{aligned} K(\omega\cos\theta, \omega\sin\theta) &= \int_{-\infty}^{\infty} e^{2\pi i\omega\rho} (\mathcal{R}k)(\rho,\theta)\, d\rho \\ &= \int_{-\infty}^{\infty} e^{2\pi i\omega\rho} \frac{\sqrt{1+4u^2}}{2t} g(u,t)\, d\rho. \end{aligned}$$

From (58) we can rewrite this as

$$\begin{aligned} &= \int_{-\infty}^{\infty} e^{2\pi i\omega \frac{t^2-u^2}{\sqrt{1+4u^2}}} \frac{\sqrt{1+4u^2}}{2t} g(u,t) \frac{2t}{\sqrt{1+4u^2}}\, dt \\ &= e^{-2\pi i \frac{\omega u^2}{\sqrt{1+4u^2}}} \int_{-\infty}^{\infty} e^{2\pi i \frac{\omega}{\sqrt{1+4u^2}} t^2} g(u,t)\, dt \\ &= e^{-2\pi i \frac{(\omega\cos\theta)^2}{4\omega\sin\theta}} G(u, \omega\sin\theta). \end{aligned} \tag{62}$$

By letting $\alpha = \omega\cos\theta$ and $\beta = \omega\sin\theta$ we obtain

$$K(\alpha,\beta) = e^{-\pi i \frac{\alpha^2}{2\beta}} G(-\frac{\alpha}{2\beta}, \beta) \tag{63}$$

provided that $\omega \neq 0$. Note that in (63) we have obtained the same expression as in (51), confirming the earlier result.

Calculating the Inverse by the Normal Radon Transform

Examining the derivation of the CRT and its relationship with the normal Radon transform above leads us to the following series of resamplings and Fourier transforms as an alternative to the ones in Section 6.1. Firstly, scale $g(u,t)$ to determine the normal Radon transform of $k(\rho,\theta)$ using (58) by defining the resampled function $h(\rho,\theta)$,

$$h(\rho,\theta) = \frac{1}{2\sin\theta\sqrt{\frac{\rho}{\sin\theta} + \frac{1}{4\tan^2\theta}}}\, g\left(\frac{-1}{2\tan\theta}, \sqrt{\frac{\rho}{\sin\theta} + \frac{1}{4\tan^2\theta}}\right), \tag{64}$$

so then

$$(\mathcal{R}k)(\rho,\theta) = h(\rho,\theta)$$

by (61). Next, we invert the normal Radon transform $(\mathcal{R}k)(\rho,\theta)$ to obtain $k(x,r)$ by one of the methods outlined in Section 2.1, *i.e.* ,

$$k(x,r) = (\mathcal{R}^{-1}(\mathcal{R}k))(x,r).$$

Then we can resample $k(x,r)$ to obtain $f(x,y)$ by

$$f(x,y) = y\, k(x, x^2+y^2).$$

7 Properties of the Circular Radon Transform

In this section we examine a number of properties of the CRT. These include the effect of translation of the target function in the transform domain, and the CRT and inverse CRT (ICRT) of some simple functions. These properties are important because we will use them later to suggest further new methods for SAR image formation.

7.1 Translations

Firstly, note that the translation in x corresponds to a translation in u in the transform domain from the definition (22) so that

$$(\mathcal{R}_c f(x - x_i, y))(u, t) = g(u - x_i, t), \tag{65}$$

where $(\mathcal{R}_c f(x, y))(u, t) = g(u, t)$. Note that this applies for all $f(x, y)$.

Next, let us consider the effect of translation perpendicular to the imaging trajectory. Let us consider a disc as our target function $f(x, y)$, but this time displaced from the origin along the y axis (Figure 3),

$$f(x, y) = \begin{cases} 1 & \text{if } x^2 + (y - y_i)^2 \leqslant r^2 \\ 0 & \text{otherwise.} \end{cases}$$

This target function is radially symmetric, which simplifies considerations for the moment.

Figure 3 also shows the circular integration path of radius t centred at $(u, 0)$ intersecting the disc centred at $(0, y_i)$. It is clear from this diagram that the resulting path integral is equivalent to that obtained from a disc centred at the origin integrated along a path centred on $(\sqrt{u^2 + y_i^2}, 0)$. Consequently, for radially symmetric target functions, we may write

$$(\mathcal{R}_c f(x, y - y_i))(u, t) = g(\sqrt{u^2 + y_i^2}, t). \tag{66}$$

For target functions that are not radially symmetric, clearly the target function imaged at $(0, y_i)$ has undergone a rotation with respect to that imaged at the origin. The rotation is through an angle of $\psi = -\tan^{-1} \frac{y_i}{u}$ which changes with slow-time u. Then we can write

$$(\mathcal{R}_c f(x, y - y_i))(u, t) = g_{-\tan^{-1} \frac{y_i}{u}}(\sqrt{u^2 + y_i^2}, t) \tag{67}$$

where $g_\psi(u, t)$ is a function of ψ as well as u, t, and is the transform of the rotated target function given by

$$g_\psi(u, t) = (\mathcal{R}_c f(x \cos\psi + y \sin\psi, -x \sin\psi + y \cos\psi))(u, t). \tag{68}$$

Consequently, to determine the CRT of a target function translated along the y-axis, we need to know its CRT at all rotations ψ when it lies on the x-axis.

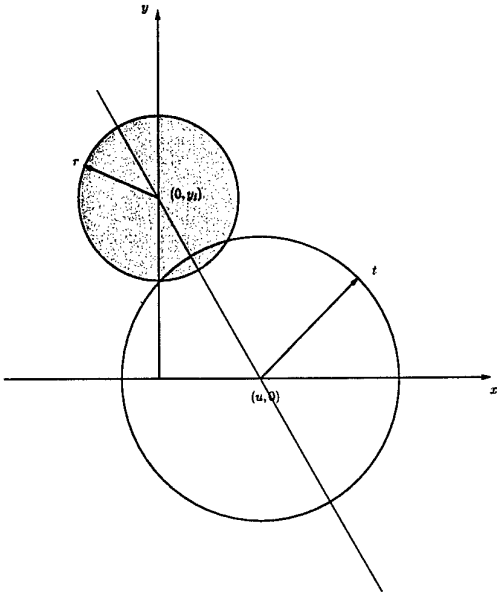

Figure 3: The geometry of a disc displaced from the origin along the y-axis, perpendicular to the imaging trajectory.

7.2 Analytic Forward Transforms

In this section we explore a number of different analytic expressions for the forward circular Radon transform.

7.2.1 Delta Function

Let our target function be the delta function located in the (x, y) plane at the point $(0, y_i)$. Then we may write

$$f(x, y) = \delta(x)\delta(y - y_i),$$

where $\delta(\cdot)$ is the Dirac delta function. The CRT of the delta function is then given by

$$\begin{aligned} g(u, t) &= \int_0^{2\pi} f(u + t\cos\theta, t\sin\theta)t\, d\theta \\ &= \int_0^{2\pi} \delta(u + t\cos\theta)\delta(t\sin\theta - y_i)t\, d\theta, \end{aligned}$$

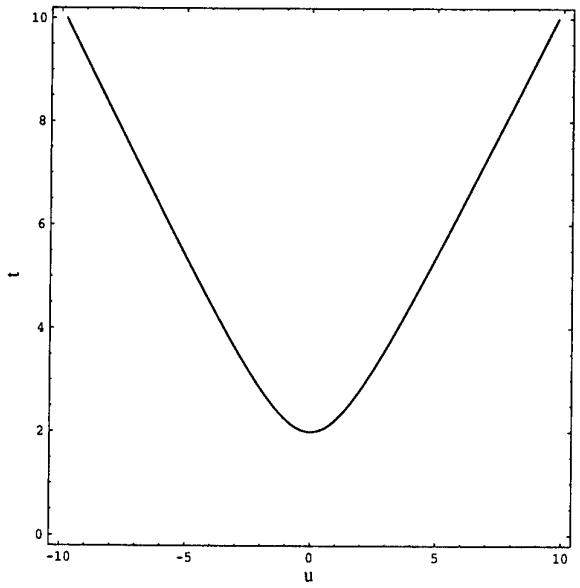

Figure 4: The trace of the circular Radon transform of a Dirac delta function at $(0, 2)$. *The weighting function on the implicit curve in (70) is not shown.*

then from Papoulis [28], $\delta(\alpha(t)) = \sum_i \frac{\delta(t-t_i)}{|\alpha'(t_i)|}$, where t_i are the zeros of $\alpha(t)$,

$$
\begin{aligned}
&= \int_0^{2\pi} \frac{\delta(\theta - \cos^{-1}\frac{-u}{t})}{t \sin\cos^{-1}\frac{-u}{t}} \frac{\delta(\theta - \sin^{-1}\frac{y_i}{t})}{t\cos\sin^{-1}\frac{y_i}{t}} t\, d\theta \\
&= \frac{1}{t\sqrt{\left(1-\frac{u^2}{t^2}\right)\left(1-\frac{y_i^2}{t^2}\right)}} \int_0^{2\pi} \delta(\theta - \cos^{-1}\frac{-u}{t})\delta(\theta - \sin^{-1}\frac{y_i}{t})\, d\theta \qquad (69)
\end{aligned}
$$

then solving $\cos^{-1}\frac{-u}{t} = \sin^{-1}\frac{y_i}{t}$ for t and taking the positive root we obtain

$$
g(u,t) = \begin{cases} \dfrac{1}{t\sqrt{\left(1-\frac{u^2}{t^2}\right)\left(1-\frac{y_i^2}{t^2}\right)}} & \text{if } t = \sqrt{u^2+y_i^2} \\ 0 & \text{otherwise.} \end{cases} \qquad (70)
$$

Figure 4 shows a plot of the trace swept out by the CRT of the delta function. Note the hyperbolic shape, which is characteristic of the CRT of finite or concentrated objects in the (x, y) plane.

7.2.2 Disc

Let us consider a disc centred on the origin, with its circumference given by

$$x^2 + y^2 = r^2.$$

We wish to determine the CRT of this disc for irradiating circles of radius t centred on the x-axis at the point $(u, 0)$. To do this, we need to determine the length of the arc of the circle that intersects the disc.

Let $g(u,t)$ denote the resulting CRT of the disc. In the case where $|u| > |r+t|$, the circle will not intersect the disc, and $g(u,t) = 0$ in such circumstances (Figure 5(a)). When $|u| = |r+t|$, there is a non-enveloping osculation between the disc and the circle (Figure 5(b)), but because the intersection between the two occurs at an infinitely small point, $g(u,t) = 0$. When $|r-t| < |u| < |r+t|$, intersection occurs between the circle and disc (Figure 5(c)), and the length of the intersecting arc is given by $g(u,t) = 2t\cos^{-1}\left(\frac{u^2+t^2-r^2}{2tu}\right)$. The enveloping osculation occurs when $|u| = |r-t|$ and $t \leqslant r$ (Figure 5(d)), and the entire circle lies within the disc, *i.e.* , $g(u,t) = 2\pi t$. If $|u| = |r-t|$ and $t = r$ then the circle lies on the circumference of the disc and $g(u,t) = 2\pi t$. If $|u| < |r-t|$ and $t \leqslant r$ then the circle is completely enveloped by the disc and $g(u,t) = 2\pi t$ (Figure 5(e)). However, if $|u| \leqslant |r-t|$ and $t > r$ then the circle envelopes the disc and $g(u,t) = 0$, intersecting at most at a single point when $|u| = |r-t|$.

In summary, the CRT of the disc centred at the origin is given by

$$g(u,t) = \begin{cases} 2t\cos^{-1}\left(\frac{u^2+t^2-r^2}{2tu}\right) & \text{if } |r-t| < |u| < |r+t|, \\ 2\pi t & \text{if } |u| \leqslant |r-t| \text{ and } t \leqslant r, \\ 0 & \text{otherwise.} \end{cases} \tag{71}$$

Figure 6 shows a density plot of the CRT of a disc of radius one. Figure 7 shows the effect of translation along the y-axis on the transform of a disc of radius one.

7.2.3 Gaussian Radial Basis Function

Let the Gaussian radial basis function (RBF) be defined by

$$f(x,y) = e^{-\pi(x^2+y^2)}. \tag{72}$$

Then the CRT of $f(x,y)$ from (22) is given by

$$g(u,t) = (\mathcal{R}_c f)(u,t) = \int_0^{2\pi} f(u + t\cos\theta, t\sin\theta)\, t\, d\theta \tag{73}$$

$$= 2\pi t e^{-\pi(t^2+u^2)} I_0(2\pi t u), \tag{74}$$

where $I_0(\cdot)$ is the modified Bessel function of the first kind of order 0. Figure 8 shows a density plot of the CRT of the Gaussian radial basis function.

We can check the effect of translation of the Gaussian RBF along the y-axis to confirm the relationship in (66) for radially symmetric target functions. Figure 3 shows the geometry of the problem. If we denote the $-\tan^{-1}\frac{y_i}{u}$ rotated coordinate system (x', y') centred on $(0, y_i)$ in the (x,y) plane with x' axis passing through the x-axis at $x = u$, then we can rewrite the Gaussian RBF function as $f(x', y') = e^{-\pi(x'^2+y'^2)}$. The centre of our integrating circle is located at $(\sqrt{u^2+y_i^2}, 0)$ in the rotated coordinate system, so then the

CRT of $f(x, y)$ from (22) is given by

$$g(u,t) = \int_0^{2\pi} f(\sqrt{u^2 + y_i^2} + t\cos\theta, t\sin\theta)t\, d\theta,$$

which integrated gives that

$$g(u,t) = (\mathcal{R}_c f(x, y - y_i))(t,u) = 2\pi t e^{-\pi(t^2+u^2+y_i^2)} I_0(2\pi t\sqrt{u^2 + y_i^2}).$$

Figure 9 shows the effect of translation along the y-axis on the transform of the Gaussian RBF.

7.2.4 Vertical Line

Let our target function be the vertical line at $x = 0$. Then we may write

$$f(x,y) = \delta(x).$$

The CRT of the vertical line is then given by

$$\begin{aligned} g(u,t) &= \int_{-\infty}^{\infty}\int_{-\infty}^{\infty} f(x,y)\delta(t - \sqrt{(x-u)^2 + y^2})\, dx\, dy \\ &= \int_{-\infty}^{\infty}\int_{-\infty}^{\infty} \delta(x)\delta(t - \sqrt{(x-u)^2 + y^2})\, dx\, dy. \end{aligned}$$

Following Papoulis [28], the angle of the intersection of the two line masses $\delta(x)$ and $\delta(t - \sqrt{(x-u)^2 + y^2})$ is given by

$$\sin\theta = \sqrt{1 - \frac{u^2}{t^2}},$$

and so the density at each intersection is $1/\sqrt{1 - \frac{u^2}{t^2}}$. Therefore,

$$g(u,t) = \begin{cases} \frac{2}{\sqrt{1-\frac{u^2}{t^2}}} & \text{if } |u| < t \\ 0 & \text{otherwise.} \end{cases}$$

7.2.5 Vertical Line Segment

Let our target function be the vertical line segment at $x = 0$ in the interval $y \in [y_0, y_1]$ where $0 \leqslant y_0 < y_1$. Then we may write

$$f(x,y) = \begin{cases} \delta(x) & \text{if } y_0 \leqslant y \leqslant y_1 \\ 0 & \text{otherwise.} \end{cases}$$

The CRT of the vertical line segment is then given by the expression

$$g(u,t) = \begin{cases} \frac{1}{\sqrt{1-\frac{u^2}{t^2}}} & \text{if } \sqrt{u^2 + y_0^2} \leqslant t \leqslant \sqrt{u^2 + y_1^2} \\ 0 & \text{otherwise.} \end{cases}$$

using the density at the intersection calculated in Section 7.2.4. Figure 10 shows a density plot of the CRT of a vertical line segment.

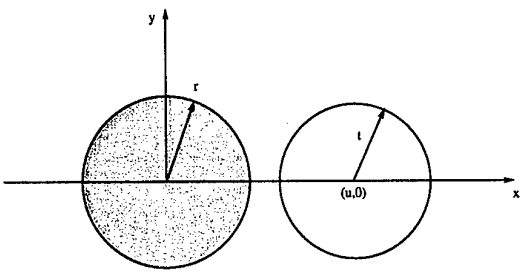

(a) Non-enveloping non-intersecting: $|u| > |r + t|$

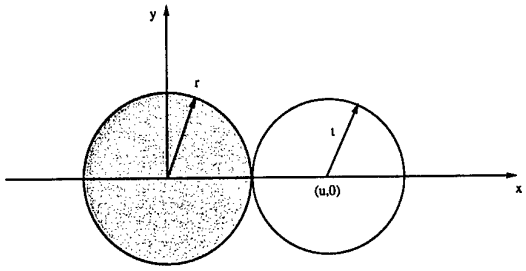

(b) Non-enveloping osculation: $|u| = |r + t|$

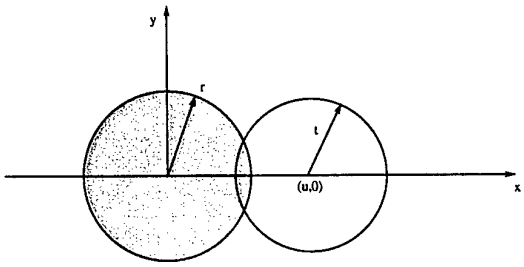

(c) Intersecting: $|r - t| < |u| < |r + t|$

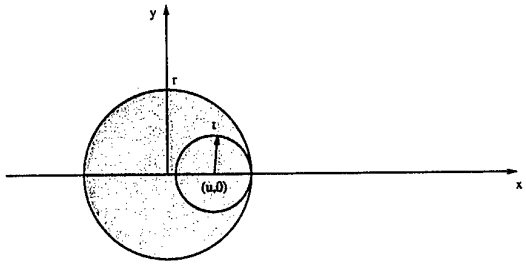

(d) Enveloping osculation: $|u| = |r - t|$ and $t \leqslant r$

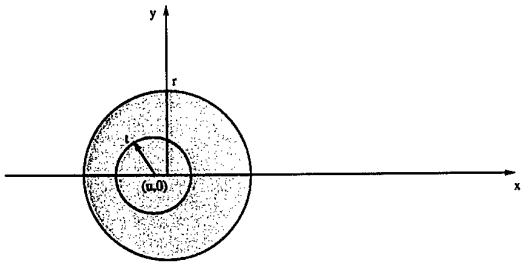

(e) Enveloping: $|u| < |r - t|$ and $t \leqslant r$

Figure 5: The various cases under which a circle can intersect a disc.

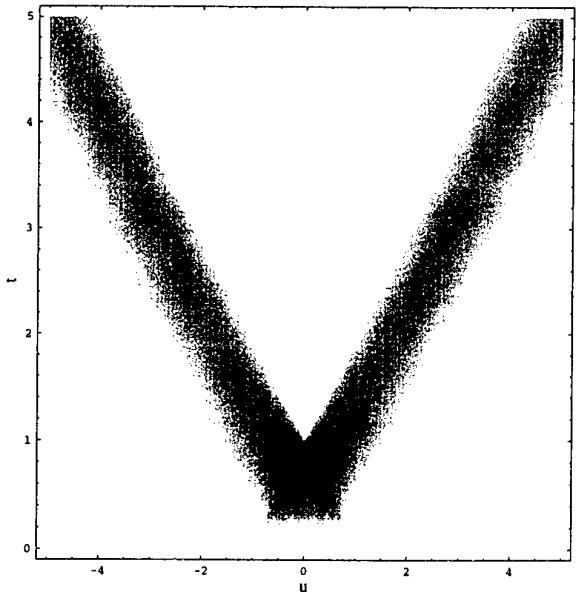

Figure 6: The circular Radon transform of a disc of radius one centred at the origin.

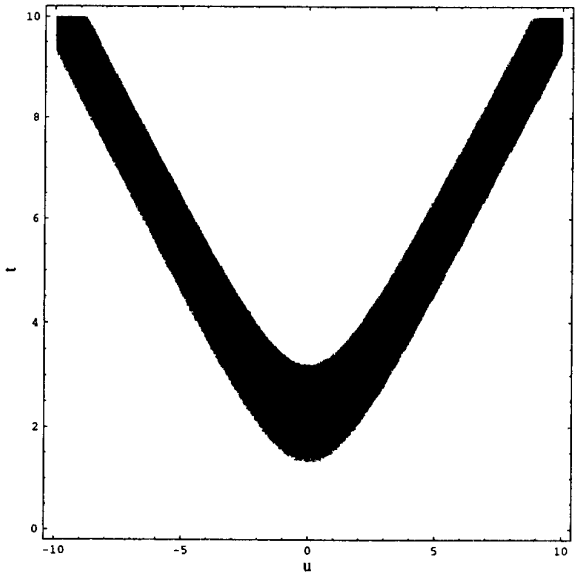

Figure 7: The CRT of a disc of radius one displaced from the origin along the y-axis to be centred on $y = \sqrt{5}$.

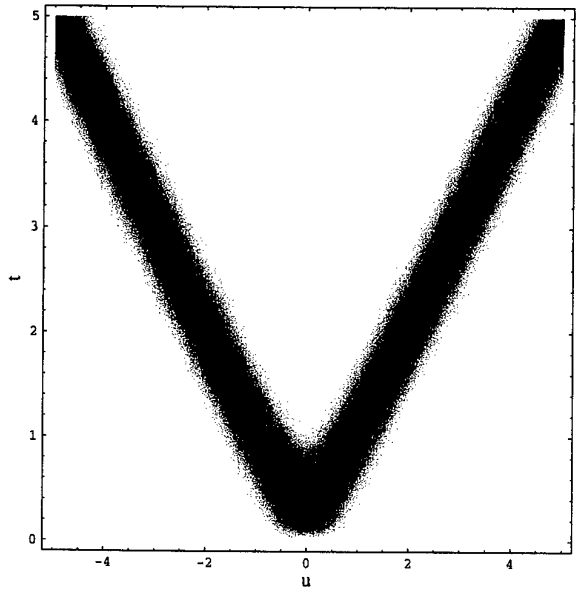

Figure 8: The circular Radon transform of a Gaussian radial basis function centred at the origin.

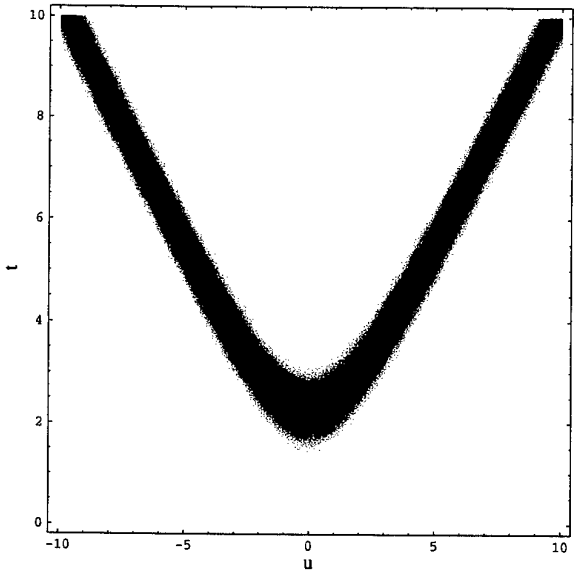

Figure 9: The CRT of a Gaussian radial basis function displaced from the origin along the y-axis to be centred on $y = \sqrt{5}$.

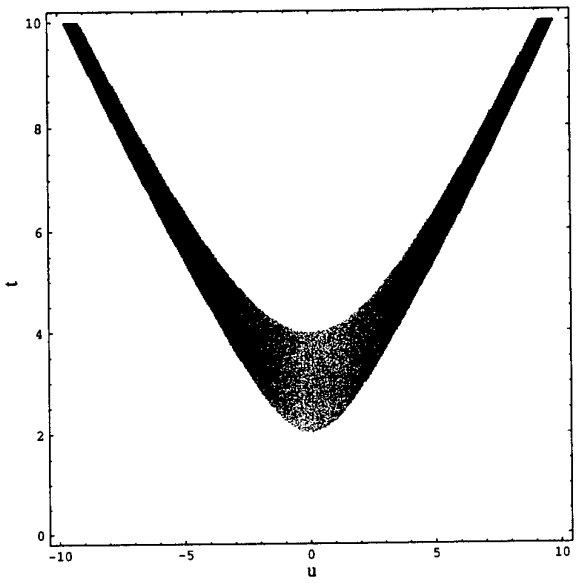

Figure 10: The CRT of a vertical line segment in the interval $y_0 = 2, y_1 = 4$.

7.2.6 Horizontal Line

Let our target function be the horizontal line at $y = y_i$. Then we may write

$$f(x, y) = \delta(y - y_i).$$

The CRT of the horizontal line is then given by

$$\begin{aligned} g(u,t) &= \int_{-\infty}^{\infty}\int_{-\infty}^{\infty} f(x,y)\delta(t - \sqrt{(x-u)^2 + y^2})\,dx\,dy \\ &= \int_{-\infty}^{\infty}\int_{-\infty}^{\infty} \delta(y - y_i)\delta(t - \sqrt{(x-u)^2 + y^2})\,dx\,dy. \end{aligned}$$

Following Papoulis [28], the angle of the intersection of the two line masses $\delta(y - y_i)$ and $\delta(t - \sqrt{(x-u)^2 + y^2})$ is given by

$$\sin(\frac{\pi}{2} - \theta) = \cos\theta = \frac{|u|}{t},$$

and so the density at each intersection is $\frac{t}{|u|}$. Therefore,

$$g(u,t) = \begin{cases} 2\frac{t}{|u|} & \text{if } t > y_i \\ 0 & \text{otherwise.} \end{cases}$$

7.2.7 Horizontal Line Segment

Let our target function be the horizontal line segment at $y = y_i$ in the interval $x \in [x_0, x_1]$ where $x_0 < x_1$. Then we may write

$$f(x, y) = \begin{cases} \delta(y - y_i) & \text{if } x_0 \leqslant x \leqslant x_1 \\ 0 & \text{otherwise.} \end{cases}$$

The CRT of the horizontal line segment is then given by the expression

$$g(u,t) = \begin{cases} \text{if } u \geqslant x_1\text{:} & \begin{cases} \frac{t}{|u|} & \text{if } (u-x_1)^2 + y_i^2 \leqslant t^2 \leqslant (u-x_0)^2 + y_i^2 \\ 0 & \text{otherwise} \end{cases} \\ \text{if } u \leqslant x_0\text{:} & \begin{cases} \frac{t}{|u|} & \text{if } (u-x_0)^2 + y_i^2 \leqslant t^2 \leqslant (u-x_1)^2 + y_i^2 \\ 0 & \text{otherwise} \end{cases} \\ \text{if } x_0 < u < x_1\text{:} & \begin{cases} 0 & \text{if } t \leqslant y_i \\ 2\frac{t}{|u|} & \text{if } (u-x_0)^2 + y_i^2 \geqslant t^2 \text{ and } (u-x_1)^2 + y_i^2 \geqslant t^2 \\ \frac{t}{|u|} & \text{if } (u-x_0)^2 + y_i^2 < t^2 \text{ and } (u-x_1)^2 + y_i^2 \geqslant t^2 \\ \frac{t}{|u|} & \text{if } (u-x_0)^2 + y_i^2 \geqslant t^2 \text{ and } (u-x_1)^2 + y_i^2 < t^2 \\ 0 & \text{if } (u-x_0)^2 + y_i^2 < t^2 \text{ and } (u-x_1)^2 + y_i^2 < t^2, \end{cases} \end{cases} \tag{75}$$

using the density at the intersection calculated in Section 7.2.6. Figure 11 shows the geometric configurations that contribute to the cases in (75). Figure 12 shows a density plot of the CRT of the horizontal line segment.

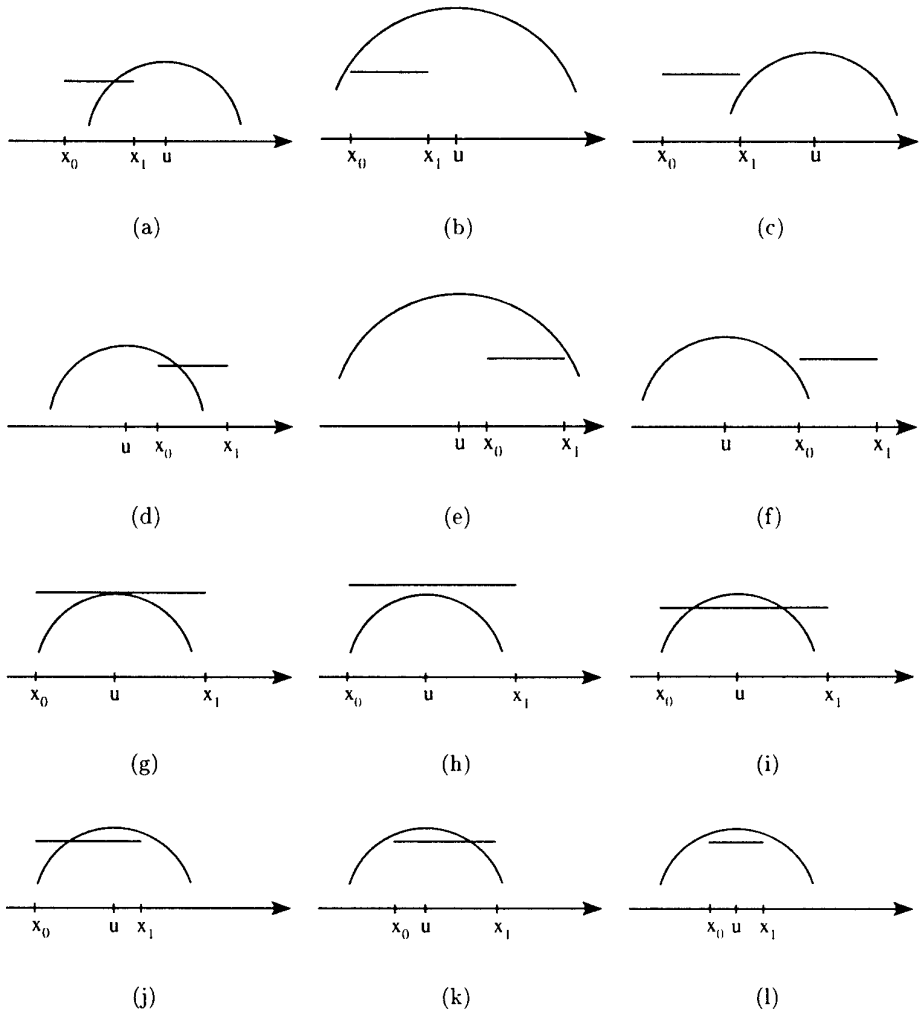

Figure 11: The various cases under which a circle can intersect a horizontal line segment.

7.2.8 Simple Polynomials and Other Functions

Table 1 presents the CRT and SCRT of a number of simple target functions. Note that $Si(\cdot)$ is the sine integral, defined to be

$$Si(z) = \int_0^z \frac{\sin t}{t}\, dt.$$

7.3 Analytic Inverse Transforms

In this section we will use the resampling transforms presented in Section 6.1 to derive the inverse CRT for target functions with known CRT.

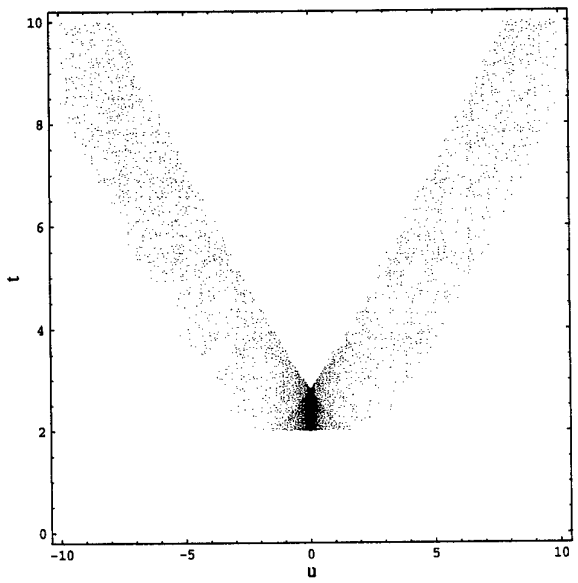

Figure 12: The CRT of a horizontal line segment $y_i = 2$ in the interval $x_0 = -2, x_1 = 2$. A square-root mapping to compress the grey scale has been used in this density plot to make the "arms" visible.

7.3.1 Bessel Function

Let our target function be the CRT of the Gaussian radial basis function in (72),

$$g(u,t) = 2\pi t e^{-\pi(t^2+u^2)} I_0(2\pi tu). \tag{76}$$

Firstly, note that $g(u,t)$ is odd in the second variable t, so we assume that $g(u,t) = 0$ for $t < 0$. Then following the steps presented in Section 6.1, from (52) and (53),

$$\begin{aligned} G(u,\omega) &= 2\pi \int_{-\infty}^{\infty} e^{2\pi i\omega t^2} t e^{-\pi(t^2+u^2)} I_0(2\pi tu)\, dt \\ &= 2\pi e^{-\pi u^2} \int_0^{\infty} t e^{\pi t^2(2i\omega-1)} J_0(2\pi itu)\, dt, \end{aligned}$$

then using (6.631.4) from [13],

$$G(u,\omega) = \frac{e^{\frac{2\pi i\omega u^2}{1-2i\omega}}}{1-2i\omega}.$$

Then from (54),

$$\begin{aligned} K(\alpha,\beta) &= e^{-\pi i\frac{\alpha^2}{2\beta}} G(-\frac{\alpha}{2\beta},\beta) \\ &= \frac{e^{-\frac{\pi\alpha^2}{1-2i\beta}}}{1-2i\beta}. \end{aligned}$$

$f(x,y)$	$(\mathcal{R}_c f)(u,t)$	$(\mathcal{R}_{c/2} f)(u,t)$
a	$2a\pi t$	$a\pi t$
ax	$2a\pi tu$	$a\pi tu$
ay	0	$2at^2$
ax^2	$a\pi t(t^2+2u^2)$	$\frac{1}{2}a\pi t(t^2+2u^2)$
ay^2	$a\pi t^3$	$\frac{1}{2}a\pi t^3$
ax^2+by^2	$\pi(at^3+bt^3+2atu^2)$	$\frac{1}{2}\pi(at^3+bt^3+2atu^2)$
axy	0	$2at^2u$
ax^3	$a\pi t(3t^2u+2u^3)$	$\frac{1}{2}a\pi t(3t^2u+2u^3)$
ay^3	0	$\frac{4}{3}at^4$
ax^2y	$a\pi t^3u$	$\frac{1}{2}a\pi t^3u$
axy^2	0	$at^2(\frac{2}{3}t^2+2u^2)$
$\frac{a}{x}$	$\frac{2a\pi t}{t+u}\sqrt{\frac{u+t}{u-t}}$	$\frac{a\pi t}{t+u}\sqrt{\frac{u+t}{u-t}}$
$\frac{a}{x^2}$	$\frac{2a\pi tu}{(t-u)^2(t+u)}\sqrt{\frac{u-t}{u+t}}$	$\frac{a\pi tu}{(t-u)^2(t+u)}\sqrt{\frac{u-t}{u+t}}$
$\frac{\sin(\pi\theta-\frac{\pi}{2})}{\pi\theta-\frac{\pi}{2}}$	$\frac{t}{\pi}(Si(\frac{\pi}{2})-Si(\frac{\pi}{2}-2\pi^2))$	$\frac{t}{\pi}(Si(\frac{\pi}{2})-Si(\frac{\pi}{2}-\pi^2))$

Table 1: The CRTs and SCRTs of a number of simple functions.

Then from (55),

$$\begin{aligned} k(x,r) &= \int_{-\infty}^{\infty}\int_{-\infty}^{\infty} e^{-2\pi i\alpha x}e^{-2\pi i\beta r}K(\alpha,\beta)\,d\alpha\,d\beta \\ &= \int_{-\infty}^{\infty} e^{-2\pi i\beta r}\left(\int_{-\infty}^{\infty} e^{-2\pi i\alpha x}\frac{e^{-\frac{\pi\alpha^2}{1-2i\beta}}}{1-2i\beta}\,d\alpha\right)d\beta \\ &= \int_{-\infty}^{\infty} \frac{e^{-2\pi i\beta r}}{1-2i\beta}\left(\int_{-\infty}^{\infty} e^{-\pi(2i\alpha x+\frac{\alpha^2}{1-2i\beta})}\,d\alpha\right)d\beta, \end{aligned}$$

then using (3.323.2) from [13],

$$
\begin{aligned}
&= \int_{-\infty}^{\infty} \frac{e^{-2\pi i\beta r}}{1-2i\beta} \left(\sqrt{1-2i\beta}\, e^{-\pi x^2(1-2i\beta)} \right) d\beta \\
&= \int_{-\infty}^{\infty} \frac{e^{-2\pi i\beta r - \pi x^2(1-2i\beta)}}{\sqrt{1-2i\beta}}\, d\beta \\
&= e^{-\pi x^2} \int_{-\infty}^{\infty} \frac{e^{-2\pi i\beta(r-x^2)}}{\sqrt{1-2i\beta}}\, d\beta \\
&= e^{-\pi x^2} \frac{e^{-\pi(r-x^2)}}{\sqrt{r-x^2}} \\
k(x,r) &= \frac{e^{-\pi r}}{\sqrt{r-x^2}}.
\end{aligned}
$$

Using (56),

$$
\begin{aligned}
f(x,y) &= y\, k(x, x^2+y^2) \\
&= e^{-\pi(x^2+y^2)},
\end{aligned}
$$

which agrees with (72).

8 Options for Inverting the Circular Radon Transform

In this report so far we have presented two equivalent methods in Section 6 for inverting the CRT *via* resampled Fourier transforms. In this section we discuss a number of options by which this inversion could be implemented. In addition, we present ideas for another novel method that uses an approximation to the fast-time matched filtered radar signal *via* a linear combination of analytic circular Radon transformed signals.

8.1 Resampled Fourier Methods

In Section 6.1, we presented a succession of resamplings and Fourier transforms that invert the CRT. There are a number of different ways of implementing this inversion, which we will now discuss.

1. The most obvious approach to take is to undertake the implementations using the FFT algorithm in conjunction with interpolation to a uniform grid after each resampling. This is a relatively simple approach, but not particularly efficient because interpolation is generally computationally intensive.

2. Two of the three interpolation steps could be eliminated by using non-uniformly sampled FFT algorithms [3, 4, 11, 29, 33, 37], which have computational complexity of the order of the standard FFT.

3. A combination of linear approximation and analytic expressions can be used to remove the need to compute some of the resampled Fourier transforms. For example, in the first step of Section 6.1, we compute

$$G(u,\omega) = \int_{-\infty}^{\infty} e^{2\pi i\omega t^2} g(u,t)\, dt.$$

If we approximate $g(u,t)$ by a sum of Gaussian radial basis functions,

$$g(u,t) = \sum_{i=i}^{n} c_i e^{-\pi \frac{(t-t_i)^2+(u-u_i)^2}{2\sigma^2}},$$

where for the moment we assume that $\sigma^2 = 1/2$, then we can write

$$\begin{aligned} G(u,\omega) &= \sum_{i=i}^{n} c_i \int_{-\infty}^{\infty} e^{-\pi((t-t_i)^2+(u-u_i)^2)} e^{2\pi i\omega t^2}\, dt \\ &= \sum_{i=i}^{n} c_i \frac{e^{-\pi((u-u_i)^2+\frac{2t_i^2\omega}{2\omega+i})}}{\sqrt{1-2i\omega}}. \end{aligned}$$

Following the next step,

$$\begin{aligned} k(x,r) &= \int_{-\infty}^{\infty}\int_{-\infty}^{\infty} e^{-2\pi i\alpha x} e^{-2\pi i\beta r} K(\alpha,\beta)\, d\alpha\, d\beta \\ &= \int_{-\infty}^{\infty}\int_{-\infty}^{\infty} e^{-2\pi i\alpha x} e^{-2\pi i\beta r} e^{-\pi i\frac{\alpha^2}{2\beta}} G(-\frac{\alpha}{2\beta},\beta)\, d\alpha\, d\beta \\ &= \int_{-\infty}^{\infty}\int_{-\infty}^{\infty} e^{-2\pi i\alpha x} e^{-2\pi i\beta r} \sum_{i=i}^{n} c_i \frac{1}{\sqrt{1-2i\beta}} e^{-\pi(u_i^2+\frac{2t_i^2\beta}{2\beta+i}+\frac{u_i\alpha}{\beta}+\frac{(1+2i\beta)\alpha^2}{4\beta^2})}\, d\alpha\, d\beta \\ &= \int_{-\infty}^{\infty} e^{-2\pi i\beta r} \sum_{i=i}^{n} c_i \frac{1}{\sqrt{1+\frac{1}{4\beta^2}}} e^{-2\pi i\frac{(t_i^2-u_i^2+2u_ix)\beta+i(2t_i^2+2u_i^2-4u_ix+2x^2)\beta^2+4x^2\beta^3}{1+4\beta^2}}\, d\beta, \end{aligned} \tag{77}$$

where the integral (77) cannot be computed analytically and so must be carried out by some numerical means such as quadrature or by sampling the Fourier transform integrand and using the FFT. There are many other possible choices of basis function apart from the Gaussian radial basis function used in this example, and many other combinations of analytical and numerical steps could be employed to implement the resampled Fourier methods of Section 6.

8.2 Linear Combination Method

In this section, we develop an idea for SAR image formation that is the logical extension of the third idea presented in the previous subsection. The idea is to approximate the fast-time slow-time signal as a linear combination of the transformed basis, and then the reconstructed image is the same weighted sum of the original basis because the CRT is a linear transform. The practical impediments to this approach are that in a real system,

only a portion of the transformed signal is observed because of the finite extent of the antenna beam pattern. The portion of transformed basis function observed will depend on the angle to the centre of the swath and the antenna pattern.

We start out by considering the Gaussian RBF transform pair,

$$\begin{aligned} f(x,y) &= e^{-\pi\frac{x^2+(y-y_i)^2}{2\sigma^2}} \\ g(u,t) = (\mathcal{R}_c f)(u,\dot{t}) &= \int_0^{2\pi} f(u+t\cos\theta, t\sin\theta)t\,d\theta \\ &= 2\pi t e^{-\pi\frac{t^2+u^2+y_i^2}{2\sigma^2}} I_0\left(\pi\frac{t\sqrt{u^2+y_i^2}}{\sigma^2}\right), \end{aligned} \tag{78}$$

where σ is the width of the Gaussian RBF. Now (78) describes an hyperbolic shape with a finite cross-section (an hyperbolic ensemble (Figure 9)), which would approach (70), the CRT of a delta function, in the limit as σ goes to zero (to a constant multiple). We need to determine the portion of the hyperbolic ensemble that is relevant to a particular imaging geometry and antenna combination.

The average squint angle (off trajectory) of a target and its observed angular extent (dictated by the distance to target, beam width, and antenna steering) will determine the interval $[u_0, u_1]$ over which the CRT of the target will be observed. If the target area is small enough, this can be assumed to be constant for all targets across the target area. Next, we determine the weighted sum of translates of the windowed version of (78) that best matched the received signal. Finally, the reconstructed image is given by the same weighted sum of the same translates of the Gaussian RBF. There are many details yet to be sorted out, however, to make this approach a practical one.

Note that in this suggested approach, we have in broad terms substituted the stationary phase approximation of the RMA by another. However, it would be possible to control the fidelity of the new approximation to achieve any desired degree of accuracy in a natural way, something that is not possible in the stationary phase approximation.

9 Motion Compensation

We will now examine how motion compensation can be incorporated into the schemes presented here for image formation *via* inversion of the CRT.

Let us examine the effect of perturbing a sample point on the transform space data. This is one step towards our goal of developing an inversion process for arbitrary imaging trajectory. Figure 13 shows the geometry of the problem. We consider displacement perpendicular to the imaging trajectory only, because displacement along the imaging trajectory is simple to deal with as we discuss in a moment (but also see Section 7.1). From this diagram we can see the effect of the perturbation, which is to change the radius of the intersecting circle at the sample point $x = u$ along the imaging axis.

We can calculate the effect upon the intersecting circle. Let d denote the displacement from the imaging axis as in Figure 13. Then the error in t of the transform of the points

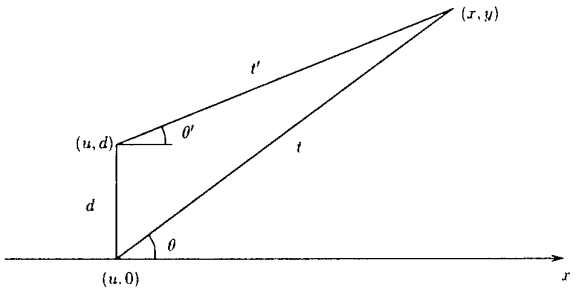

Figure 13: The geometry of a displaced point.

in the plane is given by

$$\begin{aligned} t - t' &= \sqrt{(x-u)^2 + y^2} - \sqrt{(x-u)^2 + (y-d)^2} \\ &= t - \sqrt{d^2 + t^2 - 2dt\sin\theta}. \end{aligned} \tag{79}$$

If we displace the points in the target plane along the direction θ to t', then the grid has been distorted to give that shown in Figure 14.

Motion compensation for reconstruction *via* backprojection is simply a matter of adjusting the coordinates to compensate for the platform movement,

$$\hat{f}(x_n, y_n) = \int_u s_m \left(u, \frac{2\sqrt{(x_n - u - x_e(u))^2 + (y_n - y_e(u))^2}}{c} \right) du. \tag{80}$$

More generally, motion compensation can be undertaken as follows [32]. Let our sensor platform trajectory be given by $[u + x_e(u), y_e(u)]$. Note that in standard approaches to image formation, standard FFT routines are used that require uniform sampling. Consequently, motion compensation in these cases must account for an error in the along-track direction to compensate for platform motion causing deviation from uniform slow-time sampling. However, if non-uniformly sampled FFT routines are used then this sampling is not a problem so motion compensation can be treated as an error in only the cross-track coordinate y.

Let our generic SAR signal be given by

$$s(u,t) = \sum_n \sigma_n \, p\left(t - \frac{2\sqrt{(x_n - u)^2 + y_n^2}}{c} \right).$$

Then using the shift theorem, the Fourier transform of the generic SAR signal with respect to fast-time t is

$$S(u,\omega) = P(\omega) \sum_n \sigma_n \exp\left(-4\pi i k \sqrt{(x_n - u)^2 + y_n^2} \right),$$

where $k = \omega/c$ and is called the wavenumber. Consequently, the measured SAR signal of target (x_n, y_n) in the (u,ω) domain under motion errors is

$$S_n(u,\omega) = \exp\left(-4\pi i k \sqrt{(x_n - u - x_e(u))^2 + (y_n - y_e(u))^2} \right)$$

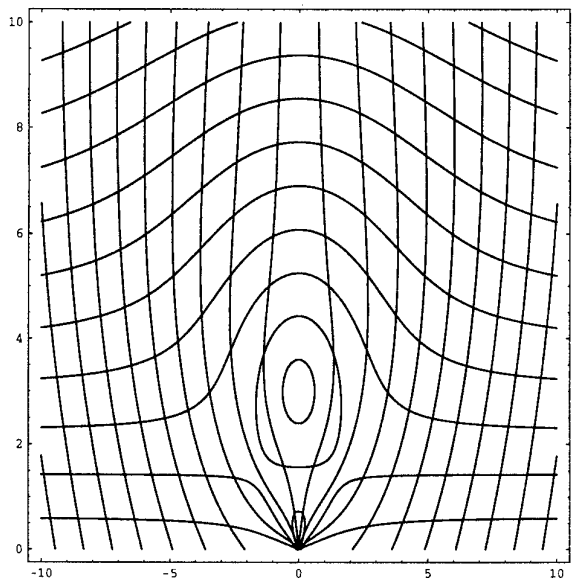

Figure 14: The distortion of the cartesian grid due to the displaced point.

where the total measured SAR signal in the (u, ω) domain is

$$S(u,\omega) = P(\omega) \sum_n \sigma_n S_n(u,\omega).$$

We can rewrite this as

$$S_n(u,\omega) = a_{en}(x_n - u, y_n, \omega) \exp\left(-4\pi i k \sqrt{(x_n-u)^2 + y_n^2}\right)$$

where the motion phase error function is given by

$$a_{en}(x_n - u, y_n, \omega) = \exp(4\pi i k r_{en}(u))$$

and the radial error for the n-th target is

$$r_{en}(u) = -\sqrt{(x_n - u - x_e(u))^2 + (y_n - y_e(u))^2} + \sqrt{(x_n-u)^2 + y_n^2}.$$

Now, provided the fluctuations of $a_{en}(x_n - u, y_n, \omega)$ are small compared with the fluctuations of $\exp\left(-4\pi i k \sqrt{(x_n-u)^2 + y_n^2}\right)$, then by the method of stationary phase ([32], p. 99) the slow-time Fourier transform of $S_n(u,\omega)$ is

$$\mathbf{S}_{en}(k_u,\omega) = A_{en}(k_u,\omega) \exp\left(-2\pi i k_u x_n - 2\pi i \sqrt{4k^2 - k_u^2}\, y_n\right),$$

where

$$A_{en}(2k\cos\theta_n(u),\omega) = a_{en}(x_n - u, y_n, \omega)$$

and the aspect angle of the n-th target when the radar is located at $(u, 0)$ is given by

$$\theta_n(u) = \tan^{-1}\left(\frac{y_n}{x_n - u}\right).$$

Now from the SAR mapping

$$k_x(k_u, \omega) = k_u$$
$$k_y(k_u, \omega) = \sqrt{4k^2 - k_u^2}$$

and the slow-time to slow-time frequency domain mapping

$$k_u = 2k\cos\theta_n(u)$$

we obtain that

$$2k = \sqrt{k_x^2 + k_y^2}$$
$$u = x_n - \frac{k_x}{k_y} y_n.$$

Therefore, $a_{en}(x_n - u, y_n, \omega)$ directly maps into the (k_u, ω) domain, and furthermore, the (k_u, ω) domain directly maps into the target spatial frequency domain (k_x, k_y). Consequently, provided that the fluctuations of $a_{en}(x_n - u, y_n, \omega)$ are small compared with the motion error-free signal, the motion phase error function $a_{en}(x_n - u, y_n, \omega)$ can be modelled as a filter in the spatial frequency domain (k_x, k_y). This filter, denoted $H_{en}(k_x, k_y)$, varies spatially with the coordinates of the target, and is given by

$$\begin{aligned} H_{en}(k_x, k_y) &= a_{en}(x_n - u, y_n, \omega) \\ &= \exp\left(4\pi i k\, r_{en}(u)\right). \end{aligned} \tag{81}$$

For narrow beamwidth SAR systems, the radial motion error function is approximated by

$$r_{en}(u) \approx x_e(u)\cos\theta_c + y_e(u)\sin\theta_c$$

where θ_c is the average squint angle (off trajectory) of the target area. Therefore, narrow beamwidth motion compensation is performed *via*

$$S_n(u, \omega)\exp\left(-4\pi i k x_e(u)\cos\theta_c - 4\pi i k y_e(u)\sin\theta_c\right), \tag{82}$$

which in the broadside case ($\theta_c = \pi/2$) simplifies to

$$-\sqrt{(x_n - u - x_e(u))^2 + (y_n - x_e(u))^2} + \sqrt{(x_n - u)^2 + y_n^2}\, S_n(u, \omega)\exp\left(-4\pi i k y_e(u)\right),$$

a filter that is independent of the position of the coordinates of the target.

In wide beamwidth systems, the assumption that the fluctuations of $a_{en}(x_n - u, y_n, \omega)$ are small compared with that of the motion error-free signal is violated. One solution is to perform narrow beamwidth compensation first using (82), which reduces the dynamic range of the errors, and then apply the shift-varying filter (81) to compensate for the remaining positional errors. After the narrow beam compensation to average squint angle θ_c, the motion error still to be compensated for is given by the expression

$$r_{exy} = -\sqrt{(x_n - u - x_e(u))^2 + (y_n - x_e(u))^2} + \sqrt{(x_n - u)^2 + y_n^2} - x_e(u)\cos\theta_c - y_e(u)\sin\theta_c.$$

10 Conclusion

The purpose of this report has been to present an alternative approach to SAR image formation from the perspective of circular Radon transforms (CRTs). This approach can naturally handle high-squint and ultra-wideband SAR. We have reviewed the literature on the inversion of circular Radon transforms, some of which has been undertaken by SAR researchers in Sweden for the CARABAS-II sensor. We present a number of novel possible approaches to the CRT inversion problem that could be developed into practical SAR image formation algorithms, and we will undertake this development in follow-on research.

11 Acknowledgements

We would like to thank Dr Mark Williams of DERA Malvern and Mark Preiss, Dr Emma Hunt, and Dr David Crisp of the Surveillance Systems Division for their helpful comments and feedback.

References

1. Agranovsky M. L., Quinto E. T., "Injectivity sets for the Radon transform over circles and complete systems of radial functions", Journal of Functional Analysis, 139, 1996, pp 383–414.

2. Andersson L.-E., "On the determination of a function from spherical averages", SIAM Journal of Mathematical Analysis, 19 (1), 1988, pp. 214–232.

3. Beylkin G., "On the fast Fourier transform of functions with singularities", Applied and Computational Harmonic Analysis, 2, 1995, pp. 363–381.

4. Beylkin G., "On applications of unequally spaced fast Fourier transforms", Mathematical Geophysics Summer School, Stanford, August 1998.

5. Bracewell R. N., The Fourier Transform and its Applications, 3rd Edition, McGraw-Hill, 2000.

6. Brandt A., Mann J., Brodski M., Galun M., " A fast and accurate multilevel inversion of the Radon transform", SIAM Journal on Applied Mathematics, 60 (2), 1999, pp. 437–462.

7. Cafforio C., Prati C., Rocca E., "SAR data focusing using seismic migration techniques", IEEE Transactions on Aerospace and Electronic Systems, 27(2), 1991, pp 194–207.

8. Carrara W. G., Goodman R. S., Majewski R. M., Spotlight Synthetic Aperture Radar Signal Processing Algorithms, Artech House, 1995.

9. Deans S. R., The Radon transform and some of its applications, 2nd Edition, Krieger Publishing Company, 1993.

10. Di Cenzo A., "A comparison of resolution for spotlight synthetic-aperture radar and computer-aided tomography", Proceedings of the IEEE, 74(8), 1986, pp. 1165–1166.

11. Duijndam A. J. W., Schonewille M. A., "Nonuniform fast Fourier transform", Geophysics, 64 (2), 1999, pp. 539–551.

12. Fawcett J. A., "Inversion of n-dimensional spherical averages", SIAM Journal of Applied Mathematics, 45 (2), 1985, pp. 336–341.

13. Gradshteyn I. S., Ryzhik I. M., Tables of Integrals, Series, and Products, Sixth Edition, Academic Press, 2000.

14. Hellsten H., Andersson L.-E., "An inverse method for the processing of synthetic aperture radar data", Inverse Problems, 3, 1987, pp. 111–124.

15. Hellsten H., "Inverse scattering analysis of diffraction limited SAR", IEEE Transactions on Antenna Propagation, 38(10), 1990, pp. 1517–1522.

16. Hellsten H., Ulander L. M. H., Gustavsson A., "Development of VHF CARABAS II SAR", Radar Sensor Technology, Proceedings of the SPIE, 2747, 1996, pp. 48–60.

17. Hochstadt H., The Functions of Mathematical Physics, Dover Publications, 1986.

18. Jakowatz C. V. Jr., Wahl D. E., Eichel P. H., Ghiglia D. C., Thompson P. A., Spotlight-Mode Synthetic Aperture Radar: A Signal Processing Approach, Kluwer Academic Publishers, 1996.

19. Lebedev N. N., Special Functions and Their Applications, Translated by R. S. Silverman, Dover Publications, 1972.

20. McCorkle J., Rofheart M., "An order $N^2 \log(N)$ backprojector algorithm for focusing wide-angle wide-bandwidth arbitrary-motion synthetic aperture radar", Radar Sensor Technology, Proceedings of the SPIE, 2747, 1996, pp. 25–36.

21. Milman A. S., "SAR imaging by ω-k migration", International Journal of Remote Sensing, 14 (10), 1993, pp 1965–1979.

22. Milman A. S., "The hyperbolic geometry of SAR imaging", submitted to IEEE Transactions on Aerospace and Electronic Systems, 2000.

23. Munson D. C., O'Brien J. D., Jenkins W. K., "A tomographic formulation of spotlight-mode synthetic aperture radar", Proceedings of the IEEE, 71(8), 1983, pp. 917–925.

24. Munson D. C., Sanz J. L. C., "Image reconstruction from frequency-offset Fourier data", Proceedings of the IEEE, 72(6), 1984, pp. 661–669.

25. Newsam G. N., Magarey J., "Multiscale Radon transform", unpublished note, 1999.

26. Nilsson S., "Application of fast backprojection techniques for some inverse problems in integral geometry", Linköping Studies in Science and Technology, Dissertations No. 499, Department of Mathematics, Linköping University, Sweden, 1997.

27. Norton S. J., "Reconstruction of a reflectivity field from line integrals over circular paths", Journal of the Acoustical Society of America, 67(3), pp. 853–863, 1980.

28. Papoulis A., "Optical systems, singularity functions, complex Hankel transforms", Journal of the Optical Society of America, 57(2), 1967, pp. 207–213.

29. Potts D., Steidl G., Tasche M., "Fast Fourier transforms for nonequispaced data: a tutorial", In: Modern Sampling Theory: Mathematica Applications, Benedetto J.J., Ferreira P. (Eds.), 1998, pp. 253–274.

30. Quinto E. T., "Radon transforms on curves in the plane", Lectures in Applied Mathematics, 30, 1994, pp 231–244.

31. Soumekh M., "A system model and inversion for synthetic aperture radar imaging", IEEE Transactions on Image Processing, 1(1), 1992, pp. 64–76.

32. Soumekh M., "Synthetic Aperture Radar Signal Processing with Matlab Applications", John Wiley & Sons, 1999.

33. Steidl G., "A note on fast Fourier transforms for nonequispaced grids", Advances in Computational Mathematics, 9, 1998, pp. 337–352.

34. Toft P., "The Radon Transform Theory and Application", PhD Thesis, Department of Mathematical Modelling, Technical University of Denmark, 1996.

35. Ulander L. M. H., Frölind P. O., Martin T., "Processing and calibration of ultra-wideband SAR data from CARABAS-II", Proceedings of the CEOS SAR Workshop, Toulouse, 26–29 October 1999, pp. 273–278.

36. Ulander L. M. H., Hellsten H., Stenström G., "Synthetic-aperture radar processing using fast factorised backprojection", Proceedings of the EUSAR Conference, Munich Germany, 23–25 May 2000, pp. 753–756.

37. Ware A. F., "Fast approximate Fourier transforms for irregularly spaced data", SIAM Review, 40 (4), 1998, pp. 838–856.

38. Williams M., "Thoughts on Nick's Radon transform paper", unpublished note, April 2001.

39. Zalcman L., "Offbeat integral geometry", The American Mathematical Monthly, 87(3), 1980, pp. 161–175.

DISTRIBUTION LIST

Inverting the Circular Radon Transform

Nicholas J. Redding and Garry N. Newsam

	Copy Number
DEFENCE ORGANISATION	
Task Sponsor	
Director, DIGO	1
S&T Program	
Chief Defence Scientist FAS Science Policy AS Science Corporate Management Director General Science Policy Development	2
Counsellor, Defence Science, London	3
Counsellor, Defence Science, Washington	Doc Data Sht
Scientific Adviser to MRDC, Thailand	Doc Data Sht
Scientific Adviser Joint	4
Navy Scientific Adviser	Doc Data Sht
Scientific Adviser, Army	Doc Data Sht
Air Force Scientific Adviser	5
Director Trials	6
Aeronautical and Maritime Research Laboratory	
Director, Aeronautical and Maritime Research Laboratory	7
Electronics and Surveillance Research Laboratory	
Director, Electronics and Surveillance Research Laboratory	Doc Data Sht
Chief, Surveillance Systems Division	8
Research Leader, Imagery Systems	9
Head, Image Analysis & Exploitation	10
Head, Imaging Radar Systems	11
Dr David Crisp	12
Dr Bridget Hobbs	13
Dr Emma Hunt	14
David I. Kettler	15
Dr Tim Payne	16
Mark Preiss	17
Dr Nicholas J. Redding	18 to 23
Dr Nick J. S. Stacy	24

DSTO Research Library and Archives

Library Fishermans Bend	Doc Data Sht
Library Maribyrnong	Doc Data Sht
Library Edinburgh	25 to 26
Australian Archives	27
Library, MOD, Pyrmont	Doc Data Sht
Library, MOD, HMAS Stirling	28
US Defense Technical Information Center	29 to 30
UK Defence Research Information Centre	31 to 32
Canada Defence Scientific Information Service	33
NZ Defence Information Centre	34
National Library of Australia	35

Capability Systems Staff

Director General Maritime Development	Doc Data Sht
Director General Land Development	36
Director General Aerospace Development	Doc Data Sht

Navy

SOSCI, Surface Combatants FEG Wartime Division, Maritime HQ, Garden Island	Doc Data Sht

Army

ABCA Standardisation Officer, Puckapunyal	37 to 40
SO(Science), DJFHQ(L), MILPO, Enoggera, Queensland 4057	Doc Data Sht
NPOC QWG Engineer NBCD Combat Development Wing, Puckapunyal	41

Air Force

Knowledge Staff

Director General Command, Control, Communications and Computers	Doc Data Sht
Director General Intelligence, Surveillance, Reconnaissance and Electronic Warfare	Doc Data Sht
Director General Defence Knowledge Improvement Team	Doc Data Sht

Intelligence Program

DGSTA, Defence Intelligence Organisation	42
Manager, Information Centre, Defence Intelligence Organisation	43

Acquisitions Program

Corporate Support Program

Library Manager, DLS-Canberra	44

UNIVERSITIES AND COLLEGES

Australian Defence Force Academy Library	45
Head of Aerospace and Mechanical Engineering, ADFA	46
Deakin University Library, Serials Section (M List)	47
Hargrave Library, Monash University	Doc Data Sht
Librarian, Flinders University	48

OTHER ORGANISATIONS

NASA (Canberra)	49
AusInfo	50
State Library of South Australia	51

ABSTRACTING AND INFORMATION ORGANISATIONS

Library, Chemical Abstracts Reference Service	52
Engineering Societies Library, US	53
Materials Information, Cambridge Scientific Abstracts, US	54
Documents Librarian, The Center for Research Libraries, US	55

INFORMATION EXCHANGE AGREEMENT PARTNERS

Acquisitions Unit, Science Reference and Information Service, UK	56
Library – Exchange Desk, National Institute of Standards and Technology, US	57
National Aerospace Laboratory, Japan	58
National Aerospace Laboratory, Netherlands	59

SPARES

DSTO Salisbury Research Library	60 to 64

Total number of copies: 64

DEFENCE SCIENCE AND TECHNOLOGY ORGANISATION DOCUMENT CONTROL DATA				1. CAVEAT/PRIVACY MARKING
2. TITLE Inverting the Circular Radon Transform			3. SECURITY CLASSIFICATION Document (U) Title (U) Abstract (U)	
4. AUTHORS Nicholas J. Redding and Garry N. Newsam			5. CORPORATE AUTHOR Electronics and Surveillance Research Laboratory PO Box 1500 Edinburgh, South Australia, Australia 5111	
6a. DSTO NUMBER DSTO–RR–0211	6b. AR NUMBER 011-855		6c. TYPE OF REPORT Research Report	7. DOCUMENT DATE August, 2001
8. FILE NUMBER B 9505–21–70	9. TASK NUMBER INT 99/184	10. SPONSOR DDIGO	11. No OF PAGES 43	12. No OF REFS 39
13. URL OF ELECTRONIC VERSION http://www.dsto.defence.gov.au/corporate/reports/DSTO–RR–0211.pdf			14. RELEASE AUTHORITY Chief, Surveillance Systems Division	

15. SECONDARY RELEASE STATEMENT OF THIS DOCUMENT

Approved For Public Release

OVERSEAS ENQUIRIES OUTSIDE STATED LIMITATIONS SHOULD BE REFERRED THROUGH DOCUMENT EXCHANGE, PO BOX 1500, SALISBURY, SOUTH AUSTRALIA 5108

16. DELIBERATE ANNOUNCEMENT

No Limitations

17. CITATION IN OTHER DOCUMENTS

No Limitations

18. DEFTEST DESCRIPTORS

synthetic aperture radar
image formation
Radon transform

19. ABSTRACT

In this report we show how image formation or reconstruction in synthetic aperture radar (SAR) can be viewed as the inversion of the circular Radon transform. The advantage of viewing image formation in this way is that it could be used in situations where more standard methods could fail such as high squint and ultra-wideband SAR. We examine previous work in the literature on circular Radon transforms and their inversion. Next, we present some novel techniques and analytic expressions for the transform of some key functions. We briefly consider motion compensation. Finally, we propose a number of possible methods that could be pursued to make new practical image formation algorithms.